
C
S
P

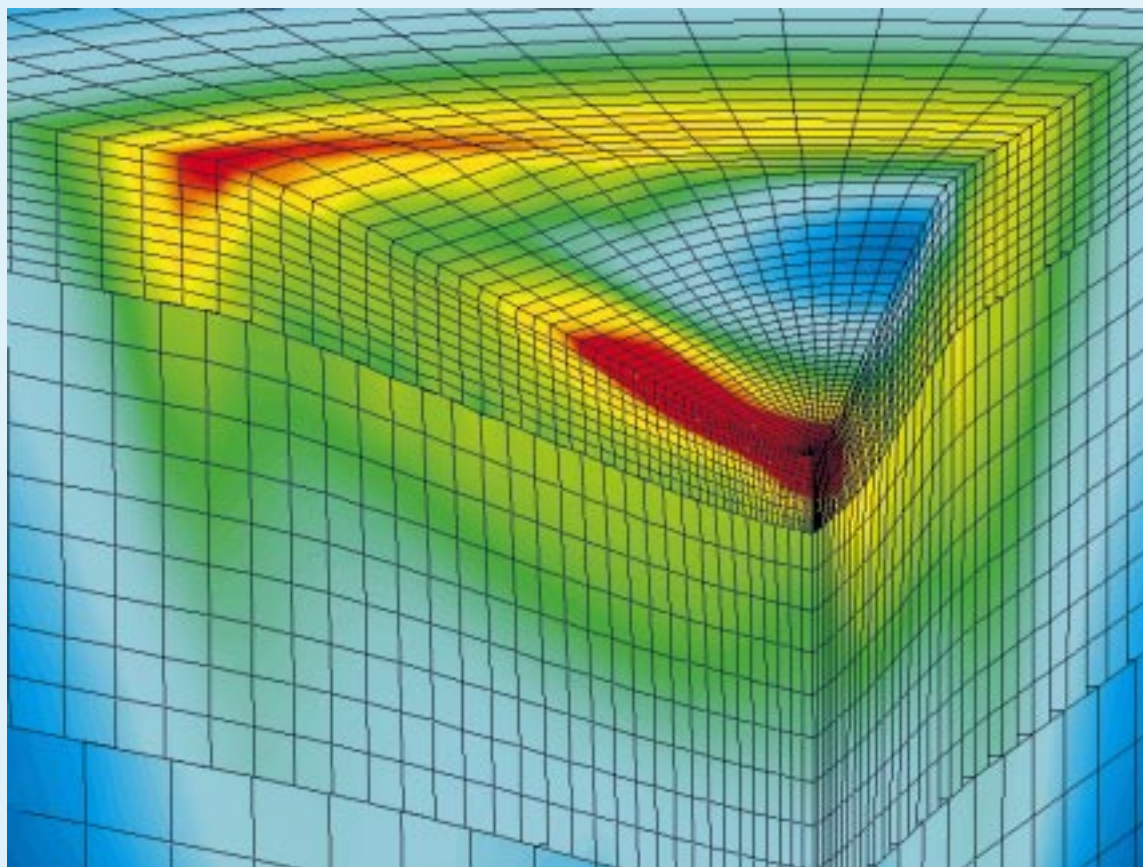
The DOE Center of Excellence for the
Synthesis and Processing
of Advanced Materials



BASIC ENERGY SCIENCES
DIVISION OF MATERIALS SCIENCE

Member Laboratories: Ames Laboratory, Argonne National Laboratory, Brookhaven National Laboratory, Idaho National Engineering and Environmental Laboratory, University of Illinois Frederick Seitz Materials Research Laboratory, Lawrence Berkeley National Laboratory, Lawrence Livermore National Laboratory, Los Alamos National Laboratory, National Renewable Energy Laboratory, Oak Ridge National Laboratory, Pacific Northwest National Laboratory, Sandia National Laboratories

Research Briefs



For questions and additional information contact:

George A. Samara
Sandia National Laboratories/NM
Phone: (505) 844-6653
Fax: (505) 844-4045
E-mail: gasamar@sandia.gov

C
S
P

The DOE **C**enter of Excellence for the
Synthesis and **P**rocessing
of Advanced Materials



BASIC ENERGY SCIENCES
DIVISION OF MATERIALS SCIENCE

Research Briefs

May 2000

Table of Contents

Preface	4
The Center's Member Laboratories	6
Membership of the Technology Steering Group	6
Center Projects and Their Coordinators	7
Executive Summary	8

Research Briefs

Metal Forming	14
• Dynamic Recrystallization During Superplastic Deformation	14
• The Material Physics of Deformation of AA5182 Under Rolling Conditions.	16
• Predicting Strength from Microstructure	18
Materials Joining	20
• Transient Liquid Phase Joining of Ceramics	20
• Electrophoretic Deposition Applied to Reaction Joining of Silicon Carbide and Silicon Nitride Ceramics	22
• Inclusion Formation in Self-Shielded Flux-Cored Arc Welds	24
• Synchrotron-Based Experimental Investigations and Numerical Modeling of Kinetics of Phase Transformations in the Heat Affected Zone of Welds	26
Microstructural Engineering with Polymers	28
• Molecularly Directed Mixing in Polymer Composite Processing	28
• Engineered Transport Properties in Polymeric Membranes	30
• Anisotropic Conductivity in Molecular Wires	32
Tailored Microstructures in Hard Magnets	34
• Improved Microstructural Control of Melt-Spun Nd ₂ Fe ₁₄ B	34

Table of Contents

• Nanocomposite Pr-Co Magnets36
• Modeling High-Performance Magnets38
Processing for Surface Hardness40
• Three-Dimensional Modeling of Nanoindentation40
• Ultrananocrystalline Diamond Thin Films42
Mechanically Reliable Surface Oxides for High-Temperature Corrosion Resistance44
• Oxide Defects and Damage Processes in Protective Alumina Films44
• Sulfur Segregation to Dynamic Al ₂ O ₃ -Metal Interfaces46
High Efficiency Photovoltaics48
• Characterizing Impurities in Thin Film Silicon48
• Ab Initio Studies of Point Defects and Dislocations in Si50
• Exciton Reduced Mass in InGaAsN Photovoltaic Materials52
Design and Synthesis of Ultrahigh-Temperature Intermetallics54
• High-Temperature Mo-12Si-8.5B Intermetallics: Fatigue and Fracture Behavior at Ambient and Elevated Temperatures54
• Oxidation Behavior of Mo ₅ Si ₃ -Based Alloys56

Preface

This publication, *Research Briefs*, is designed to inform present and potential customers and partners of the DOE Center of Excellence for the Synthesis and Processing of Advanced Materials (CSP) about significant advances resulting from Center-coordinated research. The format for *Research Briefs* is an easy-to-read, not highly technical, concise presentation of the accomplishments. Each *Brief* provides a statement of the motivation for the research followed by a description of the accomplishment and its significance.

The Center is a distributed center for promoting coordinated, collaborative research partnerships related to the synthesis and processing of advanced materials. It was established by the Department of Energy's Division of Materials Sciences, Office of Basic Energy Sciences and the DOE Laboratories in recognition of the enabling role of materials synthesis and processing to numerous materials fabrication- and manufacturing-intensive technologies. The participants include investigators from 12 DOE national laboratories, universities and the private sector. The Center has a technology perspective provided by a Technology Steering Group.

By bringing together synergistic activities and capabilities in selected focus areas of materials synthesis and processing, the Center's goal is to be a vehicle for providing added value and making impact. The Center is also allowing better coordinated strategic planning by the Division of Materials Sciences and the Laboratories and faster response time to special needs and opportunities. Additionally, the Center strives to be a model of R and D integration within the Department of Energy as well as a model of cooperation among the participating institutions.

The overall objective of the Center is,

To enhance the science and engineering of materials synthesis and processing in order to meet the programmatic needs of the Department of Energy and to facilitate the technological exploitation of materials.

Synthesis and processing (S&P) are those essential elements of Materials Science and Engineering (MS&E) that deal with (1) the assembly of atoms or molecules to form materials, (2) the manipulation and control of the structure at all levels from the atomic to the macroscopic scale, and (3) the development of processes to produce materials for specific applications. Clearly, S&P represent a large area of MS&E that spans the range from fundamental research to technology. The goal of basic

research in this area ranges from the creation of new materials and the improvement of the properties of known materials, to the understanding of such phenomena as diffusion, crystal growth, sintering, phase transitions, to the development of novel diagnostic, modeling and processing approaches, etc. On the applied side, the goal of S&P is to translate scientific results into useful materials by developing processes capable of producing high quality cost-effective products.

The technical emphasis of the Center is on a number of focused multilaboratory projects which draw on the complementary strengths of the member institutions in their ongoing research programs. These projects were selected on the basis of the following criteria:

- scientific excellence
- clear relationship to energy technologies
- involvement of several laboratories
- existing or potential partnerships with DOE Technologies-funded programs
- existing or potential "in-kind" partnerships with industry

Each Project is coordinated by a knowledgeable representative from one of the participating laboratories. The Projects covered in this issue of *Research Briefs* and their Coordinators are listed in the accompanying table (p. 7). A few selected accomplishments from each of the Projects are presented. An Executive Summary provides highlights of these accomplishments organized by Project. Readers are encouraged to contact any of the Coordinators for information about the Center and its accomplishments.

Four of the projects listed in the table on page 7, namely, Materials Joining, Tailored Microstructures in Hard Magnets, Processing for Surface Hardness and Mechanically Reliable Surface Oxides for High-Temperature Corrosion Resistance were graduated at the end of FY1999. Center Projects are graduated after achieving their objectives, but no later than five years after start. The four graduated Projects were replaced by the following four projects: Isolated and Collective Phenomena in Nanocomposite Magnets, Controlled Defect Structures in Rare-Earth Ba-Cu-O-Cuprate Superconductors, Interfacial Adhesion Related to Protective Oxides Grown on Metallic Substrates, and The Science of Localized Corrosion. Future issues of *Research Briefs* will highlight some of the accomplishments of these projects.

George A. Samara
May 2000

The Center's Member Laboratories

The member laboratories of the Center are:

- Ames Laboratory (Ames)
- Argonne National Laboratory (ANL)
- Brookhaven National Laboratory (BNL)
- Idaho National Engineering and Environmental Laboratory (INEEL)
- University of Illinois Frederick Seitz Materials Research Laboratory (UI/MRL)
- Lawrence Berkeley National Laboratory (LBNL)
- Lawrence Livermore National Laboratory (LLNL)
- Los Alamos National Laboratory (LANL)
- National Renewable Energy Laboratory (NREL)
- Oak Ridge National Laboratory (ORNL)
- Pacific Northwest National Laboratory (PNNL)
- Sandia National Laboratories (SNL)

Membership of the Technology Steering Group

<u>Member</u>	<u>Affiliation</u>
Dr. David W. Johnson, Jr.	Bell Labs, Lucent Technologies
Dr. Hylan B. Lyon	Marlow Industries
Dr. Neil E. Paton	Howmet Research Corporation
Dr. Marvin Singer	DOE/Fossil Energy
Dr. Charles Sorrell	DOE/Energy Efficiency & Renewable Energy
Dr. John Stringer	Electric Power Research Institute (EPRI)

Center Projects Covered In This Issue Of *Research Briefs* and Their Coordinators

Project	Coordinator(s)
Metal Forming	Michael Kassner (Oregon State) Phone: (541) 737-7023 FAX: (541) 737-2600 E-mail: kassner@engr.orst.edu
Materials Joining	R. Bruce Thompson (Ames) Phone: (515) 294-8152 FAX: (515) 294-7771 E-mail: thompsonrb@cnde.iastate.edu
Microstructural Engineering with Polymers	Gregory J. Exarhos (PNNL) Phone: (509) 375-2440 FAX: (509) 375-2186 E-mail: gj_exarhos@pnl.gov
Tailored Microstructures in Hard Magnets	Samuel D. Bader (ANL)* Phone: (630) 252-4960 FAX: (630) 252-9595 E-mail: bader@anl.gov
Processing for Surface Hardness	James B. Roberto (ORNL) Phone: (865) 576-0227 FAX: (865) 574-4143 E-mail: jlr@ornl.gov
Mechanically Reliable Surface Oxides for High-Temperature Corrosion Resistance	Linda L. Horton (ORNL) Phone: (865) 574-5081 FAX: (865) 574-7659 E-mail: hortonll@ma160.ms.ornl.gov
High Efficiency Photovoltaics	Satyen Deb (NREL) Phone: (303) 384-6405 FAX: (303) 384-6481 E-mail: satyen_deb@nrel.gov
Design and Synthesis of Ultrahigh-Temperature Intermetallics	Roddie R. Judkins (ORNL) Phone: (865) 574-4572 FAX: (865) 574-5812 E-mail: judkinsrr@ornl.gov and R. Bruce Thompson (Ames) Phone: (515) 294-8152 Fax: (515) 294-7771 E-mail: thompsonrb@cnde.iastate.edu
Overall Center Coordinator	George A. Samara (SNL/NM) Phone: (505) 844-6653 FAX: (505) 844-4045 E-mail: gasamar@sandia.gov

*Replaces Bob Dunlap who has retired

Executive Summary

The *Research Briefs* presented in this publication are intended to inform the Center's present and potential customers and partners about significant advances resulting from Center-coordinated research. Selected accomplishments from each of eight Center focused projects are presented. This Executive Summary states the overall objective of each project followed by highlights of the accomplishments presented later in more detail.

Metal Forming

Objective

Develop a scientific understanding of the phenomena relating to the forming of aluminum alloys for industrial (especially automotive) applications.

Highlights

- In-situ TEM has allowed direct observation of dynamic recrystallization during superplastic deformation of Al-4Mg-0.3Sc. Migration, disintegration and annihilation of subgrain boundaries were directly observed for the first time providing insight as how to tailor the microstructure to optimize the forming process.
- A technique that allows measurement of the kinetics of recrystallization for the strain rates and temperatures associated with hot rolling of Al alloys has been developed. The technique, which is based on loading a compression specimen to a given state, pausing for a specified time, and then reloading, provides information required for the development of constitutive models.
- Using TEM, key microstructural parameters such as spacing between dislocation boundaries and high angle boundaries as well as the misorientations across these boundaries, were measured on cold-rolled nickel. Analysis of the results suggest two strengthening mechanisms: (i) dislocation strengthening due to the presence of low angle boundaries, and (ii) grain boundary strengthening due to medium to high angle boundaries. Qualitatively the same dislocation structure evolution occurs in aluminum, and the same analysis can be applied.

Materials Joining

Objective

Improve the reliability of the process used to join materials into more complex structures serving a variety of energy-related functions.

Highlights

- A transient liquid metal phase process for joining ceramics which promotes interfacial dewetting of the liquid film has proven effective in producing strong joints. Using Cu/Nb/Cu multilayers, controlled dewetting of the Cu produced strong Nb/alumina bonds in joining alumina parts.
- Electrophoretic deposition combined with reaction bonding has produced fine grained, high strength SiC joints. The process is applicable for the fabrication of large, complex structures from small components of SiC and Si₃N₄.
- A thermodynamic/kinetic model has been successfully used to study the formation and evolution of nonmetallic inclusions in self-shielded flux cored arc welds in steels. The interactions between dissolved Al, Ti, N₂ and O₂ can be manipulated to induce either oxide or nitride formation as well as to control the stability of austenite or ferrite in the weld.
- In-situ spatially-and time-resolved X-ray diffraction techniques are being used to obtain the only direct observations of the phases present during welding as well as the transformation kinetics during heating and cooling of welds. Numerical modeling of the experimental data allows prediction of weld behavior beyond the experimental domain.

Microstructural Engineering with Polymers

Objective

Develop and implement novel processing methods which direct the evolution of hierarchical microstructures in composites, impart multifunctionality, and induce property changes through blending of components at the molecular level.

Highlights

- Different approaches to mixing composite precursors at the molecular level have led to significant improvements in the structure, mechanical strength and thermal stability of polymer/ceramic composites compared to conventional mixing. The improved properties make possible lighter and more versatile composites.
- Chemical modifications to inorganic polymer membranes based upon polysiloxanes or polyphosphazenes have resulted in improved performance and enhanced materials stability of rechargeable Li/LiMn₂O₄ batteries. The highly reactive chemical environment in such batteries readily degrades polymer electrolyte systems.
- An electrolytic method for the synthesis of model linear chain compounds which exhibit one-dimensional electronic conductivity due to d_z orbital overlap has been developed. Continuous polymer chain bundles with lengths approaching 30 cm and cross sections <0.5 μm in diameter based on potassium tetracyanoplatinate have been prepared.

Tailored Microstructures in Hard Magnets

Objective

Improve hard magnets by understanding, in terms of the microstructures achieved, the magnetic and mechanical properties of materials produced by a number of synthesis and processing approaches.

Highlights

- It has been demonstrated that the pressure and type of gas utilized during rapid solidification determines the overall quench rate of the $\text{Nd}_2\text{Fe}_{14}\text{B}$ liquid and thereby the microstructure of the resultant ribbon. This work defines the path for producing fine-scale, homogeneous microstructure with optimized magnetic properties.
- PrCo_5 , which spinodally decomposes below 850°C , was successfully grown in quaternary Pr-Co-Ti-C system in which carbon stabilizes the PrCo_5 and excess carbon is removed by TiC precipitation. The resulting single phase PrCo_5 in a nanoscale composite structure exhibits high values of the energy product representing 90% of the theoretical value.
- Exchange spring coupled bilayers and superlattices of magnetically hard (SmCo) and soft (Co or Fe) layers have been synthesized, characterized and modeled revealing a large increase in $(\text{BH})_{\text{max}}$ product. The insights gained define a promising new pathway to achieving stronger permanent magnets.

Processing for Surface Hardness

Objective

Understand the critical synthesis and processing issues which limit the use of plasma-based processing for surface hardness and use this understanding to improve the hardness of thin films and coatings.

Highlights

- Three dimensional finite-element modeling of nanoindentation that takes account of the actual indenter shape has been developed to quantify the mechanical properties of hard surface layers independently of those of soft substrates. Comparison of the 3-D results with our earlier 2-D modeling results on both metals and non-metals show that the 2-D simulations (which are much faster and cheaper) are quite accurate, but the 3-D results provide deeper insights into the deformation process.
- Very smooth, phase pure nanocrystalline (3-5 nm) diamond films have been successfully grown to thicknesses exceeding $30\mu\text{m}$ by a hydrogen/argon plasma-assisted CVD process. The performance of these films as coatings on SiC rotary shaft pump seals reveals exceptional wear properties compared to uncoated seals.

Mechanically Reliable Surface Oxides for High-Temperature Corrosion Resistance

Objective	<i>Generate the knowledge required to establish a scientific basis for the design and synthesis of improved (slow growing, adherent, sound) protective oxide coatings and scales on high temperature materials without compromising the requisite bulk material properties.</i>
Highlights	<ul style="list-style-type: none"> • Microstructural studies of isothermally and cyclically oxidized specimens of Fe-Al, FeCrAlY and NiCrAlY exposed for the same time and temperature failed to reveal evidence of incipient defects or damage in the grown alumina scales. The results call into question models in which defect production and damage development determine the nature of oxide spallation and the loss of oxidation resistance. • Auger electron spectroscopy results on Al₂O₃-Fe₃Al and Al₂O₃-FeCrAl interfaces revealed that the kinetics of S segregation to the interfaces depends strongly on the composition of the alloy being oxidized as well as on the oxide growth rate and the structural nature of the Al₂O₃-metal interface. Results such as these are important to the development of strategies to minimize S segregation which is believed to weaken the interfacial bond.

High Efficiency Photovoltaics

Objective	<i>Generate advances in scientific understanding that will impact the efficiency, cost and reliability of thin film photovoltaics cells by addressing short-and long-term basic research issues.</i>
Highlights	<ul style="list-style-type: none"> • Synchrotron X-ray fluorescence is being used to determine metal impurities as well as their chemical state in polysilicon and to correlate the distribution of these impurities with cell performance. Fe impurities are found to be in highly stable, hard to remove oxide and silicate forms which are likely responsible for poor performance. • Density functional theory has been used to study defect properties and their interactions with dopants in silicon. Specifically, boron was found to diffuse via an interstitialcy mechanism, and the local distortion field, relaxation volume of the Si vacancy and the reconstruction energy per bond at the core of partial dislocations were calculated. • Photoluminescence studies of the semiconductor alloy system InGaAsN at both 1 bar and high pressure have provided an understanding of the influence of the substitution of N for As on the bandgap energy and exciton effective mass, properties important for assessing the suitability of this material for use in multi-junction solar cells with efficiencies >40%.

Design and Synthesis of Ultrahigh-Temperature Intermetallics

Objective

Generate the knowledge required to establish a scientific basis for the processing and design of transition-metal silicides with improved metallurgical and mechanical properties at ambient and high temperatures. The ultimate goal is to develop scientific principles to design new-generation materials based on silicides for structural applications at and above 1400°C.

Highlights

- A combination of high fracture toughness ($>10\text{Mpa}\sqrt{\text{m}}$) with a fatigue threshold of $7\text{MPa}\sqrt{\text{m}}$ at temperatures as high as 1200°C has been demonstrated for the Mo-12Si-8.5B alloy. These results are impressive for any high-temperature intermetallic system without (expensive) composite reinforcement.
- The oxidation in air of binary and several boron-containing Mo_5Si_3 alloys was studied at $500\text{-}1400^\circ\text{C}$. Binary Mo silicides are prone to nonprotective oxidation at low temperatures ($500\text{-}700^\circ\text{C}$) primarily because the silica growth rates needed to form an external continuous scale are extremely low. The value of B addition to accelerate the formation of borosilicate is not proven.

Research Briefs

Dynamic Recrystallization During Superplastic Deformation

L. M. Dougherty and I. M. Robertson, University of Illinois
J. S. Vetrano and S. M. Bruemmer, Pacific Northwest National Laboratory
T. G. Nieh, Lawrence Livermore National Laboratory

Motivation—Superplasticity is a process by which materials can undergo extremely high elongations when deformed at high temperatures. However, deformation rates typically required for this process are too slow for high-volume applications such as the automotive industry. This research is aimed towards understanding the phenomenon of dynamic recrystallization during superplastic deformation, which can lead to an overall forming time that is shorter than the time required to form material that is statically recrystallized prior to deformation. In this brief we report on the mechanisms of dynamic recrystallization as observed in-situ by deforming specimens at the superplastic forming temperature in the transmission electron microscope (TEM). The material used was an Al-4Mg-0.3Sc alloy (similar to commercial AA5083) in which fine, coherent Al₃Sc particles stabilize the microstructure against static recrystallization.

Accomplishment—Previous research at LLNL has shown the importance of dynamic recrystallization in Al-Mg-Sc alloys by demonstrating elongations of more than 500% at the high strain rate of $1 \times 10^{-1} \text{ s}^{-1}$. This is nearly three orders of magnitude faster than normally utilized in statically recrystallized alloys. Samples of Al-4Mg-0.3Sc were deformed in tension at 460°C and a strain rate of $1 \times 10^{-3} \text{ s}^{-1}$ to true strains of 0.1 to 0.8, and quenched under load to freeze the microstructure. These strains represent the range in which the material undergoes dynamic recrystallization as determined by orientation imaging microscopy (OIM) and optical

microscopy (OM). A sample deformed to a strain of 0.2 was deformed at 460°C in-situ in the TEM. Migration, disintegration and annihilation of subgrain boundaries during the process of dynamic recrystallization were observed. Figure 1 is a schematic showing the initial configuration of two boundaries, GB1 and GB2, and dislocation arrays 1 and 2. These arrays are remnants of GB1, produced as the junction between GB1 and GB2 moved in the direction indicated in Figure 1. Each array broke free of GB1 as a unit and then moved as a unit. Figure 2a shows arrays 1 and 2 (arrow indicates direction of motion) and a reference particle A. In Figures 2b and 2c, array 1 migrates as a whole and coalesces with array 2. The newly formed array moves as a unit as shown in Figure 2d and eventually interacts with particle A and neighboring particles. These interactions cause the array to break into individual dislocations, which migrate independently and are individually accommodated in a nearby high-angle grain boundary.

Significance—The utilization of in-situ TEM has allowed direct observation of dynamic recrystallization mechanisms. Migration, disintegration and annihilation of subgrain boundaries were directly observed for the first time. Gaining a better understanding of the movement of these subgrain boundaries and their interaction with particles will allow one to tailor the microstructure to optimize this process, resulting in suitable strain rates for commercial forming of components.

Contact: John S. Vetrano, Pacific Northwest National Laboratory
Phone: (509) 372-0724, Fax: (509) 376-6308, E-mail: john.vetrano@pnl.gov

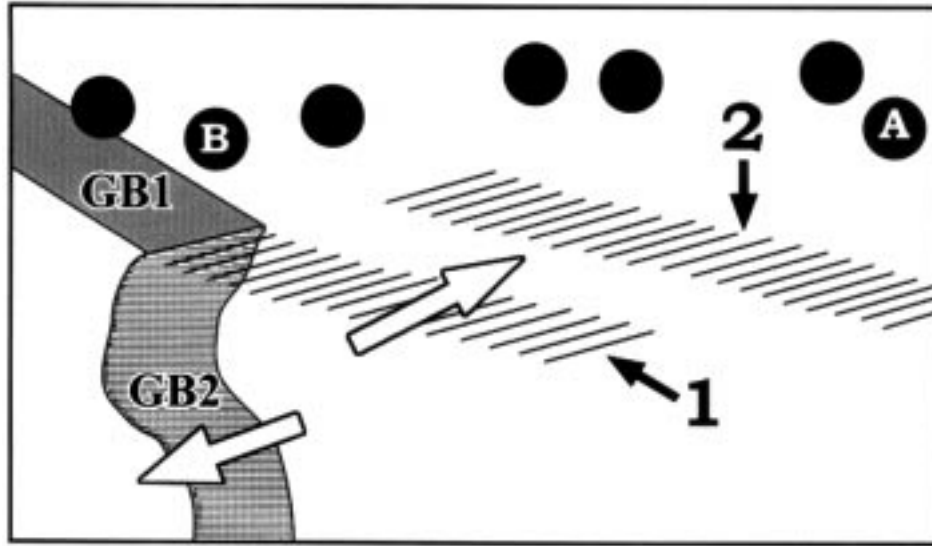


Figure 1. Schematic of the area shown in Figure 2 indicating the subgrain boundaries (GB1 and GB2), dislocation arrays (1 and 2) and particles.

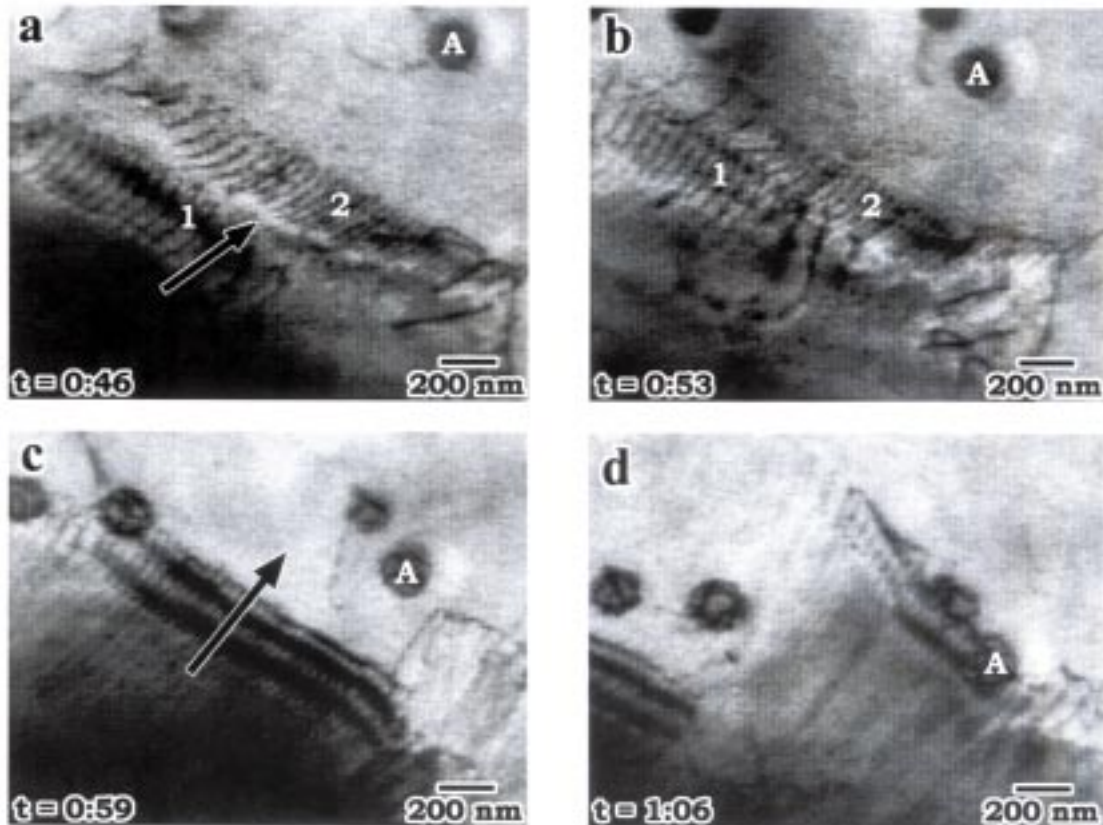


Figure 2. TEM micrographs from in-situ heating/straining experiments showing subgrain boundary coalescence (1a and 1b) and migration (1c and 1d).

The Material Physics of Deformation of AA5182 Under Rolling Conditions

M. G. Stout, Los Alamos National Laboratory, A. J. Beaudoin and M. Bange, University of Illinois, and S. R. MacEwen, Alcan International

Motivation—The forming process of hot rolling not only has obvious commercial importance but also is scientifically challenging to understand. Accurate characterization is difficult as material physics affecting plastic deformation changes on the same time scale as that of the process itself. Recovery and recrystallization provide examples: the development of an annealed state may occur between rolling passes, with subsequent impact on flow behavior in upcoming passes. To construct constitutive relations relevant to the process of hot rolling we must know when the material being rolled will recover or recrystallize as a function of strain rate and temperature. A significant challenge lies in the determination of recrystallization (static in our case) as it takes place in the same time as spent deforming our metal and faster than we can quench the sample to freeze its structure.

Accomplishment—We found that loading a AA5182 compression specimen to a given state, pausing for a particular time, and reloading the specimen gave not only constitutive information, but it allowed us to ascertain whether or not the specimen had recrystallized during the pause. The key to this understanding was plotting the materials constitutive response as hardening (Θ), i.e. $d\sigma/d\varepsilon$, vs. stress (σ). Common to all tests, Θ vs. σ plots show an initial transient followed by a linear decrease in hardening rate with stress (Vocé behavior). The stress level at which individual curves join the common curve gives indication of the restorative mechanism: recrystallized samples join at stresses \leq and recovered samples at stresses $>$ that observed for the initial curve. By varying the lengths of the pause in the loading history we were able to determine the time required for recrystallization as a function of strain rate and temperature.

The deformation of the AA5182 at a strain rate of 3.0 s^{-1} to 0.25 compressive strain at 475°C provides a specific example of this technique (see Fig. 1). One can see the close match between the initial hardening response and that from reloading after hold times of 20 and 25 s. The reload hardening after a 10 s hold is similar to these data, perhaps just a bit higher. The hardening curves after holds of 4, 2, and 1 s are distinctly higher than the loading data.

We have taken x-ray inverse pole figures of two compression specimens that were quenched after deformation to 0.25 strain at 475°C and $\dot{\varepsilon}^v=3 \text{ s}^{-1}$. The first specimen was immediately quenched and the second was held for 3 s at 475°C before quenching. A thermocouple mounted in each sample recorded their time-temperature profile. It took 7.4 and 10.9 s, respectively, for these samples to drop below 300°C in the quenching process. Temperatures above 300°C are sufficient to cause recrystallization. The inverse pole figures are shown in Figs. 2 (7.4s to 300°C) and 3 (10.9s to 300°C). The classical compression texture is (101), while that for recrystallization is (001). One can see that 7.4 s was sufficient to begin the recrystallization process. The (101) deformation texture is dramatically diminished. However, the process was not completed as there is not a distinct (001) component. In the 10.9 s case, the (001) component is present. The recrystallization is complete or nearly complete.

Significance—A technique that allows measurement of the kinetics of recrystallization for the strain rates and temperatures associated with hot rolling, which cannot be done with a quenching technique alone, was demonstrated. This provides information required to develop constitutive models.

Contact: M. G. Stout, Los Alamos National Laboratory
Phone: (505) 667-6750, Fax: (505) 665-4013, E-mail: mstout@lanl.gov

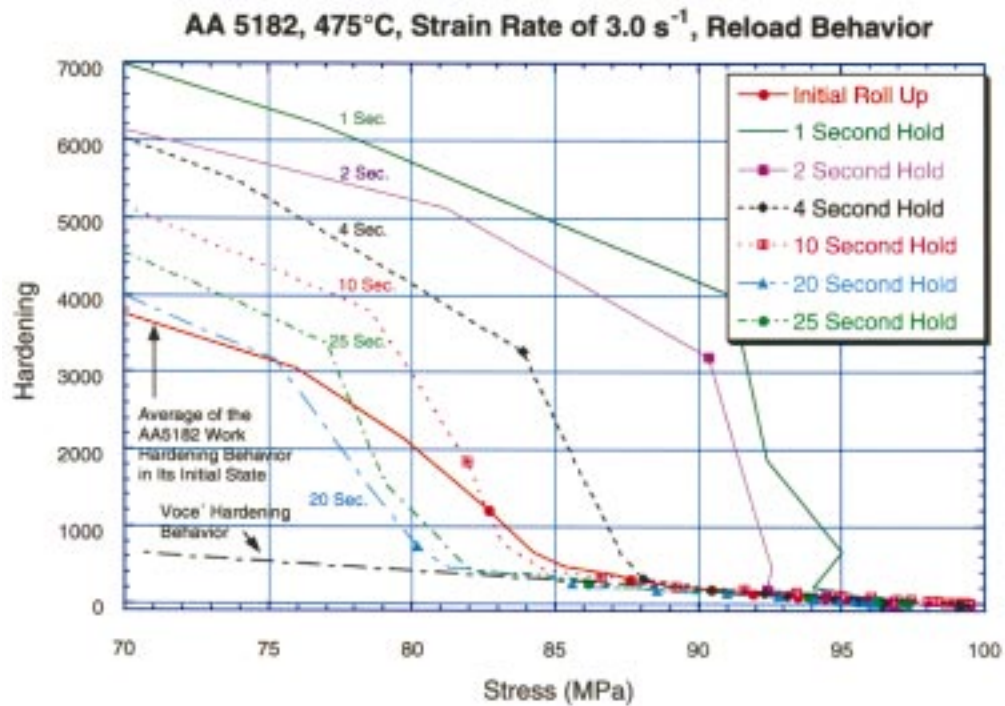


Figure 1. Constitutive response, hardening, of the AA5182. The material was loaded to a strain of 0.25 at 475°C and a strain rate of 3 s⁻¹; deformation was paused for different time increments and the sample reloaded. The reloading hardening response provides evidence for recrystallization or only thermally activated dynamic recovery during the pause.

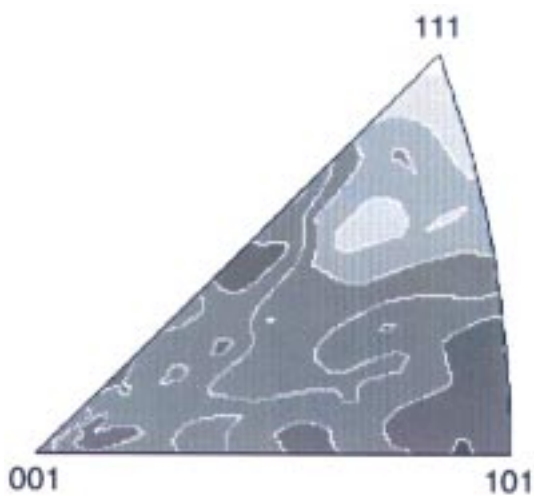


Figure 2. Inverse pole figure after 7.4 s. Note the remaining (101) deformation texture.

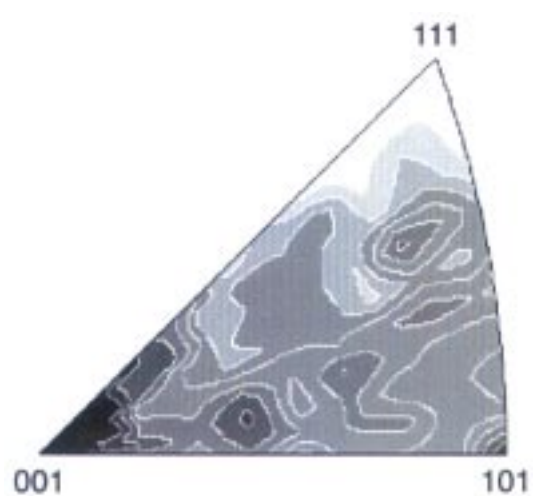


Figure 3. Inverse pole figure after 10.9 s. Note the (001) recrystallization texture.

Predicting Strength from Microstructure

D. A. Hughes, Sandia National Laboratories, Livermore CA

N. Hansen, Risø National Laboratory, Denmark

Motivation—New tools for characterizing and analyzing microstructures have been developed in the last five years which create a firmer basis to explore the relationship between microstructure and flow stress. A central question is the identification of the different microstructural elements, their relative strength contributions and persistence from small to large strain deformation.

Accomplishment—A quantitative microstructural analysis was performed on pure polycrystalline nickel (99.99%) cold rolled to reductions including 10, 20, 70, 90 and 98% (evM 0.1 to 4.5). Applying transmission electron microscopy (TEM) techniques key structural parameters, such as spacing between dislocation boundaries and high angle boundaries, as well as the misorientations across these boundaries, have been measured and analyzed. Application of scaling and similitude hypotheses to these microstructural parameters and their distributions revealed that the structures are homologous with increasing strain. This similar behavior indicates that the measured parameters capture the important features of the structure. The following conclusions are reached. The key structural element is a cell block, composed of cell block (geometrically necessary) boundaries, GNBs, and cell (incidental dislocation) boundaries, IDBs (Figure 1). For both types of boundaries, boundary spacing and width decrease and the misorientation angle increases

with increasing strain. Saturation of these parameters was not observed. Taking all the measurable structural parameters: spacing, misorientation angle, and dislocation density, and assuming additive strength contributions, we derive from Hall-Petch and dislocation strengthening flow stress predictions which are in good agreement with the stress values and hardening rates observed experimentally (Figure 2). No saturation of the calculated or experimental flow stress was observed.

Significance—Scaling and similitude provide governing principles for structure formation. Based on this structural information and a detailed description of the morphology, structural parameters are identified, strength determining parameters chosen, and strength-structural relationships obtained. The suggestion is then made that two strengthening contributions should be considered: (i) dislocation strengthening due to the presence of low angle boundaries and (ii) grain boundary strengthening due to medium to high angle boundaries. The calculated individual strength contributions evolve differently with the strain and their addition leads to flow stress values and hardening rates in good agreement with those observed experimentally. Although the results presented here are for nickel, qualitatively the same dislocation structure evolution occurs in aluminum, and the same analysis can be applied.

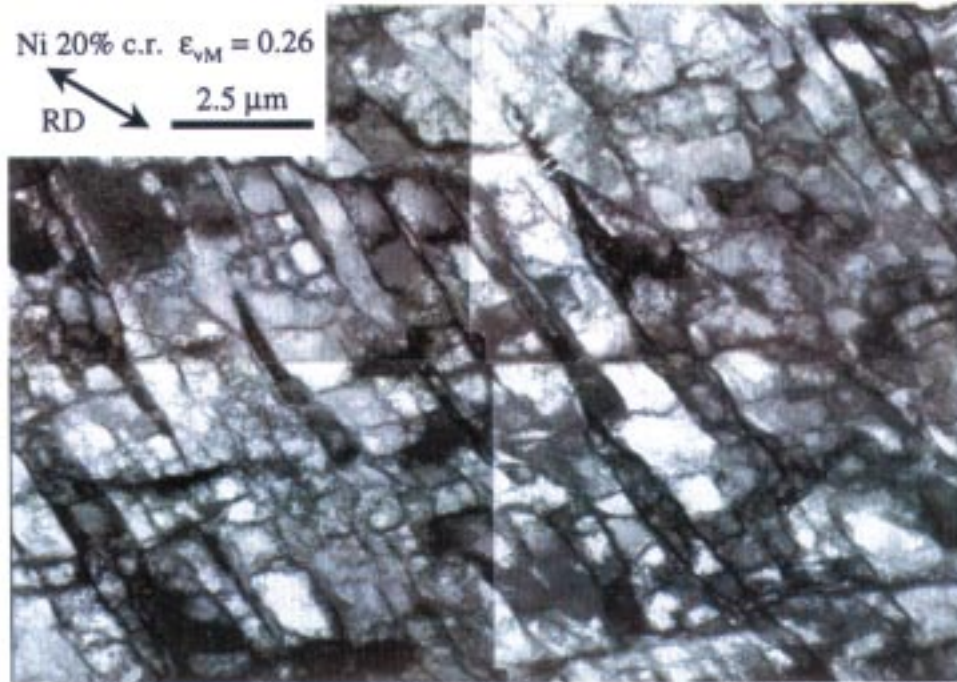


Figure 1. TEM micrograph of cold rolled pure nickel illustrating nearly planar extended GNBs surrounding more equiaxed cells to form cell blocks.

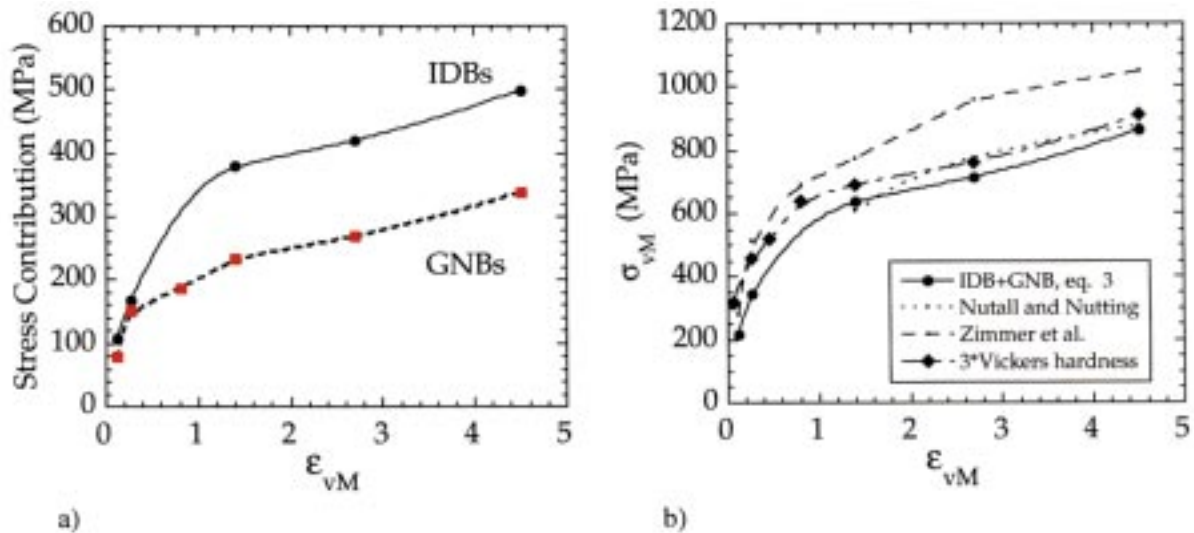


Figure 2. a) The strength contribution of IDBs is based on dislocation strengthening, while that of the GNBs is based on Hall-Petch strengthening. Both types of boundaries contribute to linear hardening at large strains above 1.5. b) Stress predictions based on the combined microstructure match the level of hardness measurements on the same samples and stress strain data from the literature. Note in particular the agreement in the strain hardening that changes from parabolic at small strain to linear at large strain.

Transient Liquid Phase Joining of Ceramics

A. M. Glaeser, Lawrence Berkeley National Laboratory

Motivation—The lack of a well-developed joining technology for ceramics limits or prevents their use in a range of applications. The problems associated with joining for high-temperature applications are particularly severe. Innovative approaches to joining different materials that overcome incompatibilities in physical properties and minimize deleterious chemical interactions are required. This research seeks to develop and apply unconventional approaches to ceramic-ceramic and ceramic-metal joining. A common theme of the methods is the utilization of microdesigned multilayer interlayers that form a thin or partial layer of a transient liquid phase (TLP) to facilitate bonding via a brazing-like process. This reduces the processing temperatures and thereby the potential for deleterious chemical interactions. Properly designed interlayers allow the use of the resulting joined assembly at temperatures that exceed the original bonding temperature, in contrast to conventionally brazed assemblies.

Accomplishment—Three approaches to TLP joining have been explored. In the first, the thin liquid layer disappears as a result of diffusion into a thicker core layer and the formation of a refractory solid solution. In the second, reactive metal penetration methods lead to the formation of a composite interlayer and disappearance of the liquid. The third promotes interfacial dewetting of the liquid film rather than its disappearance. Here a thin film of a low melting metal dewets the interface between a high melting point metal and the ceramic to be joined. Bond formation occurs by a process reminiscent of liquid-phase sintering. Copper/niobium/copper interlayers serve as an example here. Alumina and sapphire substrates were joined using multilayer copper/niobium/copper inter-

layers. Bonded assemblies of alumina produced at 1400°C and a pressure of ~2 MPa exhibited high fracture strengths ($\approx 240 \pm 20$ MPa) that approached those of the alumina used (280 ± 30 MPa), Fig. 1. Fractography of samples that failed along the interface revealed that the initially continuous layer of copper between the niobium and alumina had evolved into a set of discrete copper particles, and intimate contact between the niobium and alumina developed (Fig. 2). An interface in which niobium/alumina contact is dominant suggests that the majority of an applied load would be borne by the niobium/alumina interface. The bend strength was measured as a function of temperature. Results on the lower strength alumina, (Fig.3) indicate that useful levels of strength are retained to 1100°C, slightly above the melting temperature of copper. Moreover, some of the failures occur within the ceramic, not along the ceramic/metal interface. Recent experiments performed with a higher purity, higher strength alumina show that the ceramic/metal interfaces retain strength levels >200 MPa to temperatures of up to 1200°C.

Significance—Transient liquid phases provide controllable methods for producing strong joints between ceramic components in which processing temperatures are below the melting point of high-temperature metals in the joint. Controlled dewetting allows strong niobium/alumina joints to be produced using copper/niobium/copper interlayers. Copper dewetting in the interface allows a significant fraction of the joint to transform to niobium/alumina (instead of copper/alumina) contact which determines the joint properties. The combination of reduced temperature processing and high-temperature joint materials is a critical success of this method.

Contact: A. M. Glaeser, Lawrence Berkeley National Laboratory
Phone: (510) 486-7262, Fax: (510) 486-6086, E-mail: amglaeser@lbl.gov

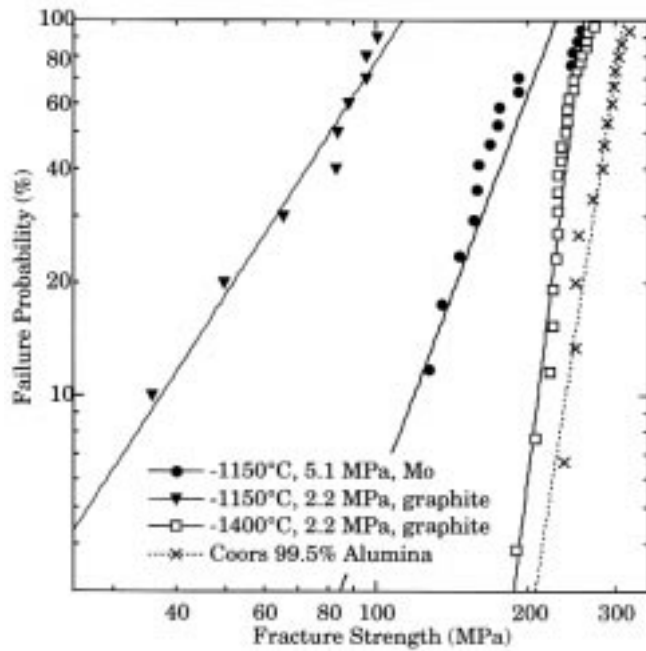
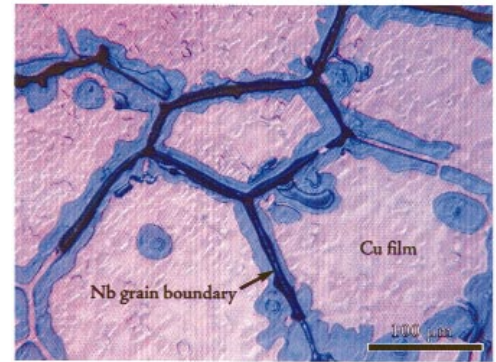
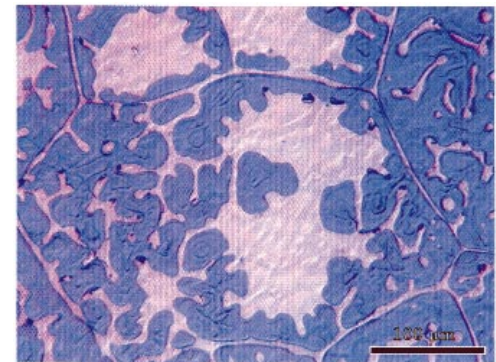


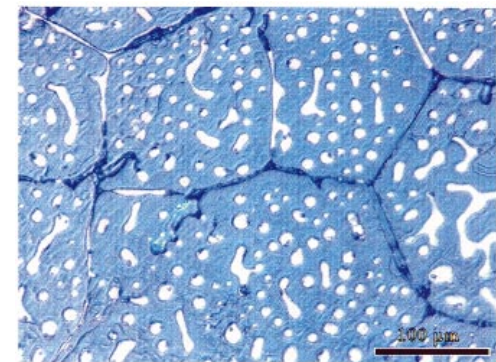
Figure 1. Plot of failure probability versus beam fracture strength illustrating effect of processing conditions on joint characteristics. Some joints were prepared in a graphite (lower oxygen partial pressure) environment, others in a molybdenum environment. The alumina reference material (Coors) was unbonded.



(a)



(b)



(c)

Figure 2. Illustration of interfacial microstructures in a sapphire/copper/niobium couple bonded at 1400°C showing possible sequence for microstructural evolution: a) initial niobium/sapphire contact along niobium grain boundary ridges, b) regression and instability of isolated copper films, and c) regions of largely niobium/sapphire contact with small isolated copper droplets.

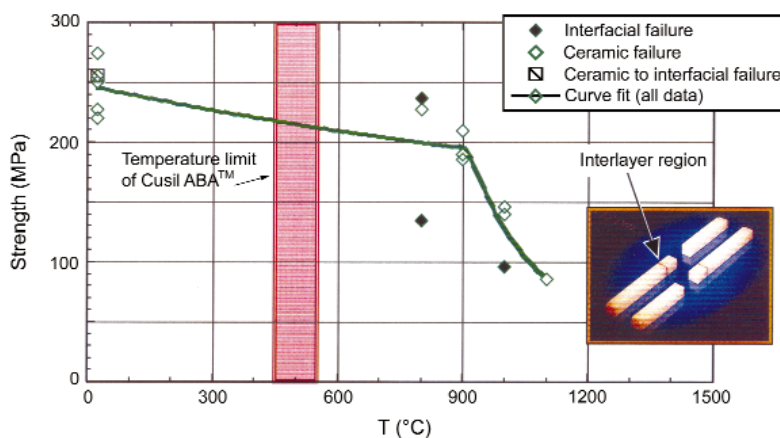


Figure 3. Plot of beam fracture strength versus temperature. Strengths are retained to high temperature, and instances of ceramic failure are observed in the 900°C-1100°C test interval. The insert shows examples of some of the higher temperature fractures.

Electrophoretic Deposition Applied to Reaction Joining of Silicon Carbide and Silicon Nitride Ceramics

Paul A. Lessing, Arnold W. Erickson, and Dennis C. Kunerth
Idaho National Engineering & Environmental Laboratory

Motivation—SiC-based ceramics and ceramic composites will be used in applications where joints are required. New and creative approaches are being investigated for this purpose since it is unlikely that one joining technology will be able to address all the critical issues in dissimilar-materials joining. Electrophoretic deposition techniques offer the ability to control and tailor the joint microstructure that is superior to established commercial technology for reaction bonding. This control should translate into superior joint performance.

Accomplishment—Electrophoretic Deposition (EPD), Fig. 1 was used to deposit a mixture of SiC or Si₃N₄ and reactive carbon (graphite and carbon black) particles onto various SiC or Si₃N₄ parts in preparation for reaction bonding. The particles had gained a surface charge when mixed into an organic liquid to form a slurry. The charged particles move under the influence of an electric field to form a "green" deposit on the ceramic parts. The parts were dried and subsequently joined using a reaction bonding method (Fig. 2). In this reaction bonding, molten Si moves into the joint via capillary action and then dissolves carbon and precipitates additional SiC. An optimum mixture of SiC "filler" to C powder ratio of 0.64 was identified. Residual Si was minimized as a result of selecting powders with controlled particle size distributions. Image analysis of resulting microstructures indicated residual Si content as low as 7.0 vol. % could be realized, which

compares favorably with the lowest residual Si levels available in experimental samples of bulk, siliconized SiC manufactured using conventional reaction-bonding techniques. The joints retained the residual silicon over a large number of high-temperature thermal cycles and did not develop cracks as the commercial material did. Ceramography indicated the majority of residual silicon of the joint was retained in closed porosity, which infers that parts made with these joints might be successfully utilized at very high temperatures. The EPD technique can be applied to butt, lap, and scarf type joints and includes the capability to fill large gaps. The overall results indicate that EPD, combined with reaction bonding, allow for the fabrication of larger, more complex structures manufactured from smaller components consisting of silicon carbide or silicon nitride.

Significance—The ability to produce fine-grained and high-strength joints between SiC-based materials has been demonstrated using a novel technology, electrophoretic deposition, originally developed to produce nano-composites. The ability to control the carbon-precursor particle size allows the process to minimize the amount of residual Si. Further, the residual Si is now in closed pores, which is advantageous in terms of residual stress and reactivity. The microstructure after reaction bonding was more stable than similar materials made using established commercial technology.

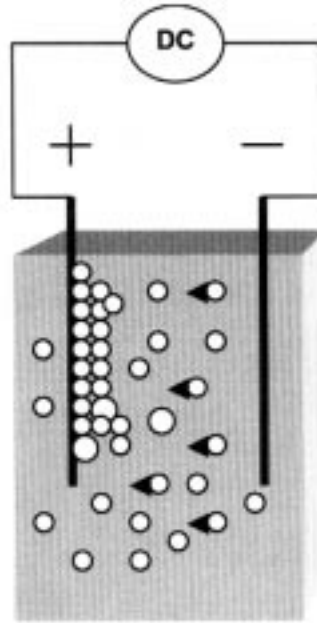


Figure 1. Schematic of EPD process.

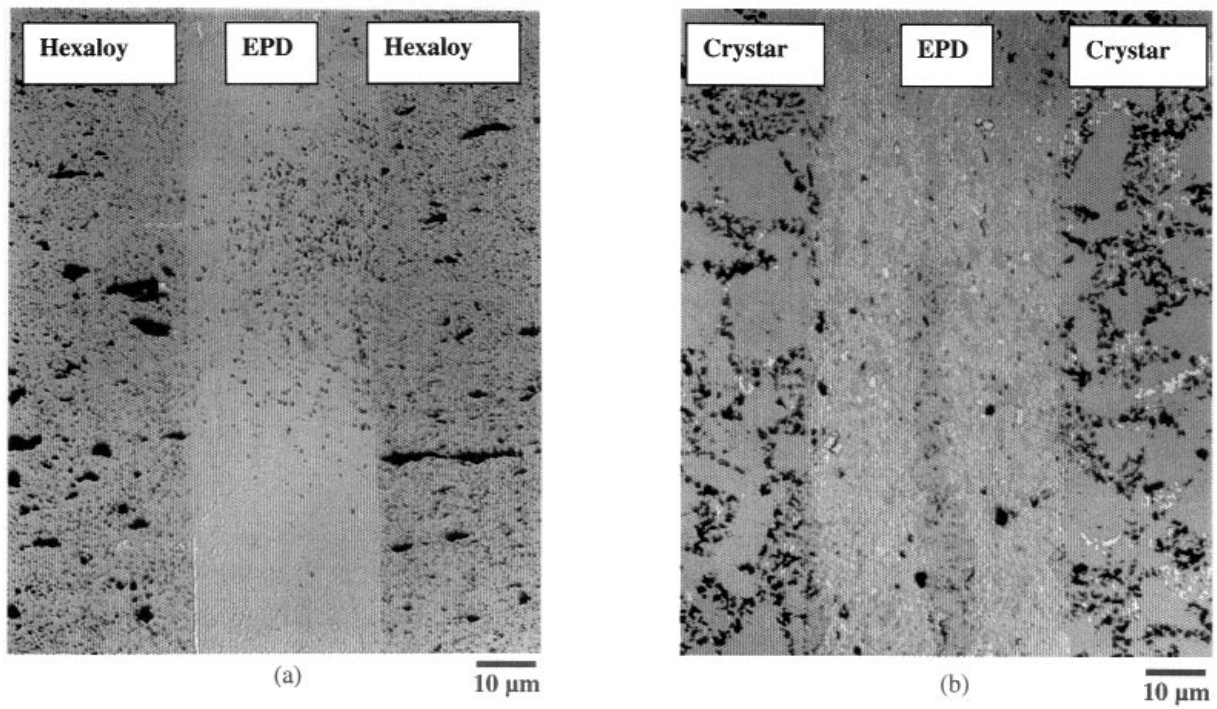


Figure 2. Optical microscopy of EPD joints. a) Hexaloy SiC tube joint, 5/8" O. D., 7° taper. b) Joined Crystar SiC pieces after 42 thermal cycles above the melting point of Si.

Inclusion Formation in Self-Shielded Flux-Cored Arc Welds

S. S. Babu, J. M. Vitek, and S. A. David, Oak Ridge National Laboratory

M. A. Quintana, Lincoln Electric Co.

J. W. Elmer, Lawrence Livermore National Laboratory

Motivation—Nonmetallic inclusions play an important role in the evolution of microstructures in steel weld metals, acting as nucleation sites for solidification and solid-state transformations on cooling and affecting mechanical properties. If present in small amounts and of the right type, they lead to better properties. In contrast, if present in large numbers and size and of undesirable type, they may decrease toughness and tensile properties. Basic understanding of the evolution of inclusions is an on-going Center research task. A thermodynamic and kinetic model has been developed at ORNL to predict the inclusion characteristics as a function of composition and welding process parameters. Here the model was applied to predict the evolution of inclusions in self-shielded flux-cored arc welds produced by Lincoln Electric Company, Cleveland, Ohio. The inclusion formation in this process is complicated due to the absence of any shielding gases, which leads to dissolution of oxygen and nitrogen from the atmosphere and subsequent reaction with metallic elements dissolved in liquid steel. The specific problem has been to identify the role of aluminum and titanium additions on the type of inclusions as well as their effect on the solidification and solid state transformations.

Accomplishment—Thermodynamic models were applied to evaluate the reaction between dissolved aluminum, titanium, oxygen, nitrogen and carbon. The stability of aluminum nitride (AlN), aluminum oxide (Al₂O₃) and titanium carbonitrides (TiCN) as a function of temperature was evaluated in two self-shielded flux-cored arc welds with two different levels of aluminum (1.7 and 0.53 wt.%) and titanium (0.003 and 0.058 wt.%) concentrations. The calculations show (see Fig. 1) that for high-

aluminum welds, as the weld cools, only AlN is the stable phase at all temperatures above the liquidus temperature. However, for low-aluminum welds, the most stable phases were found to be Al₂O₃ and TiCN and their formation overlaps as the weld cools. Characterization with transmission and scanning electron microscopy revealed that the inclusions in the weld with high-aluminum concentration were predominantly AlN. In contrast, the inclusions in welds with low-Al and high-titanium concentrations were mostly Al₂O₃ and TiCN (Fig. 2). The measurements were in excellent agreement with the predictions from the inclusion model. The predicted simultaneous formation of Al₂O₃ and TiCN was also experimentally observed as shown in Fig. 2(b). The results also show that depending upon the type of reaction, the dissolved Al levels in these welds can lead to a deleterious skeletal morphology of δ ferrite phase or to a classical high-toughness acicular ferrite.

Significance—The results show that the metal-oxygen and metal-nitrogen reactions compete with each other. Depending upon the alloy compositions, the chemical interactions between dissolved aluminum, titanium, nitrogen and oxygen elements in liquid steel can be manipulated to induce either oxide or nitride formation. The results also show that these reactions control the amount of aluminum in solid solution, which affects the stability of austenite and ferrite in these welds and thereby controls the final properties. Therefore, the present research shows a viable welding-consumable design methodology by which we can optimize both deoxidation reactions as well as the weld metal properties. In-situ X-ray diffraction and kinetic measurements are planned to study microstructure development in these welds.

Contact: S. A. David, Oak Ridge National Laboratory
Phone: (865) 574-4804, Fax: (865) 574-4928, E-mail: davidsa1@ornl.gov

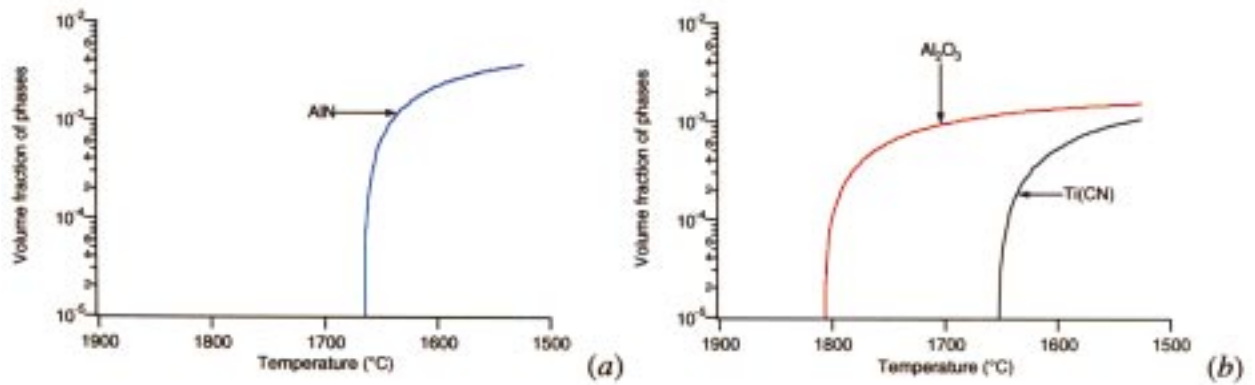


Figure 1. Equilibrium thermodynamic calculations of volume fraction of Al₂O₃, AlN, and TiCN as a function of temperature for (a) high-aluminum weld and (b) low-aluminum weld.

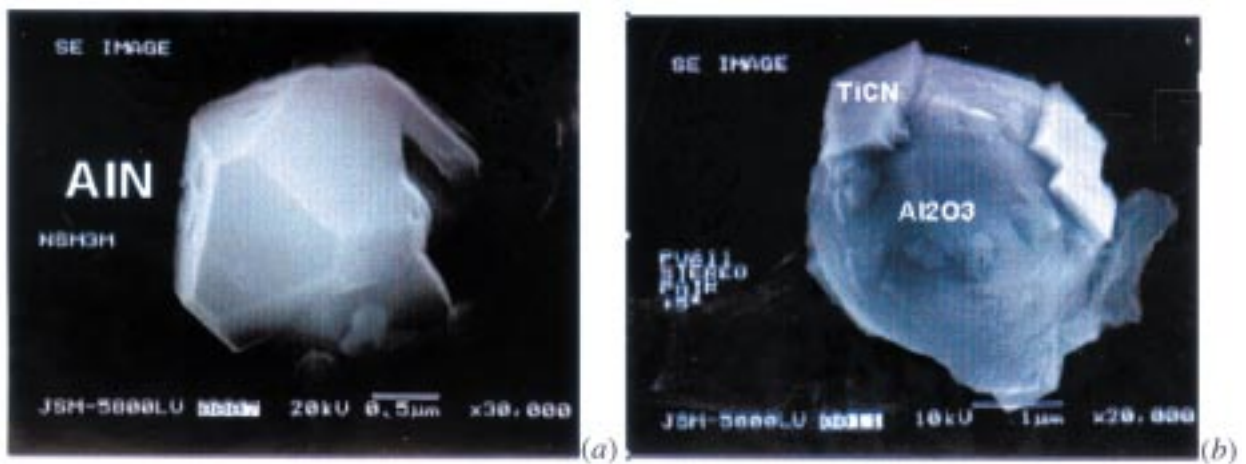


Figure 2. Scanning electron micrographs (a) showing the presence of AlN in high-aluminum welds and (b) indicating simultaneous formation of Al₂O₃ and TiCN in low-aluminum welds.

Synchrotron-Based Experimental Investigations and Numerical Modeling of Kinetics of Phase Transformations in the Heat Affected Zone of Welds

J. W. Elmer and J. Wong, Lawrence Livermore National Laboratory

T. DebRoy, Z. Yang and S. Sista, The Pennsylvania State University

S. A. David and S. Babu, Oak Ridge National Laboratory

Motivation—Spatially Resolved X-Ray Diffraction (SRXRD) and Time Resolved X-Ray Diffraction (TRXRD) methods are being developed at LLNL for in-situ investigations of phase transformations in the heat-affected zone (HAZ) of welds. In this region of the weld, severe temperature gradients, high peak temperatures and rapid thermal fluctuations occur as the heat source passes through the material. These non-isothermal temperature fluctuations produce HAZ microstructures that cannot be predicted by conventional methods. The unique synchrotron-based experiments being developed here will enable the determination of phase transformation kinetics under true non-isothermal welding conditions, and can be used to aid in the development of models to predict HAZ microstructural evolution.

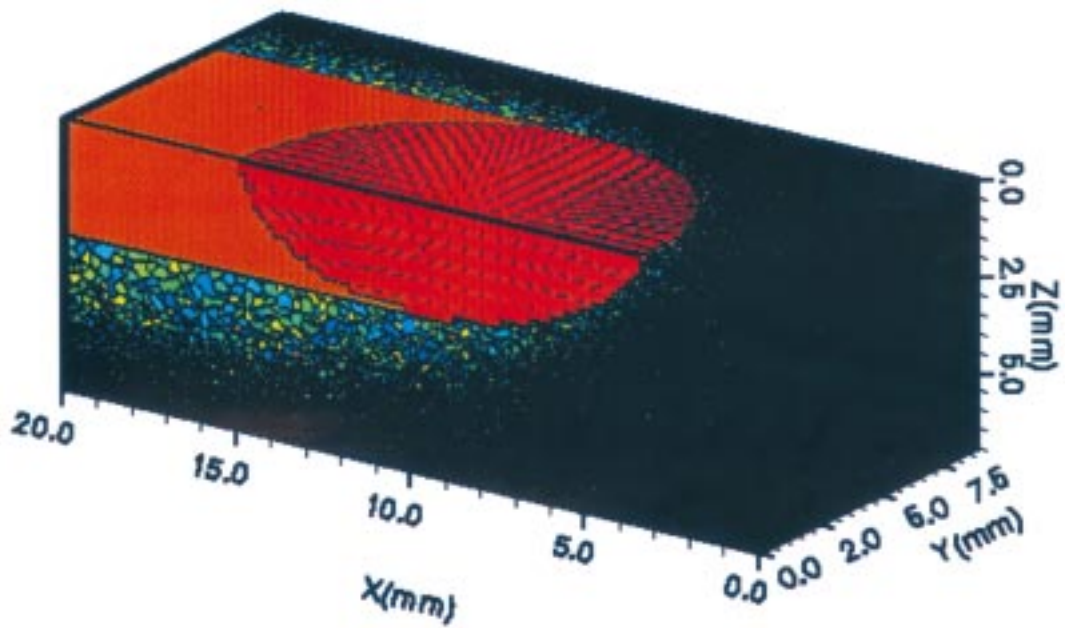
Accomplishment—SRXRD experiments on AISI type 304 stainless steel gas tungsten arc (GTA) welds were recently completed. These in-situ experiments were conducted at Stanford Synchrotron Radiation Laboratory to investigate the solidifying weld crater with time-resolved experiments (50 ms), and the HAZ with spatially resolved experiments (260 μm). Both stationary (spot) welds and moving welds were examined. Results of the spot welds showed, for the first time, that solidification occurs directly to the delta ferrite phase. After solidification to δ , the $\delta \rightarrow \gamma$ phase transformation in this stainless steel alloy was observed as the weld cooled to room temperature. In experiments on AISI 1005 carbon-manganese steel, long-range diffusion of interstitial carbon plays a major role in the transformation kinetics. The results are being analyzed, and will be used to map the regions of the ferrite, austenite and delta phases of iron in the weld HAZ. TRXRD studies are

being performed on a flux cored arc welding electrode used for welding low carbon structural steels through our collaboration with Oak Ridge National Laboratory. The TRXRD measurements on the two steel alloys are further being studied to determine if in-situ temperature measurements can be made using the shift in the diffraction peaks of the ferrite phase during heating and cooling.

The SRXRD-based phase transformation map for grade 2 titanium was analyzed with our Penn State Collaborators using a transient, 3-D, turbulent heat transfer and fluid flow model and modified Johnson-Mehl-Avrami formalism. The results successfully predicted the region of $\alpha+\beta$ coexistence around the titanium weld pool. The model was used to compare different rate controlling steps for the $\alpha \rightarrow \beta$ transformation and was used to predict the region where the complete transformation to the β phase had occurred. Real-time evolution of the grain structure in the single-phase β region of titanium was also modeled (Fig.) using a 3-D Monte Carlo technique coupled to the heat transfer and fluid flow model. This code was specifically developed to account for the steep HAZ thermal gradients that exist around the weld pool.

Significance—These XRD techniques provide the only known direct observations of the phases present during welding and can be used to measure transformation kinetics during heating and cooling of welds. Numerical modeling of the experimental data allows predictions of weld behavior over a wider range of welding parameters than is experimentally examined, and can be used to help identify the most likely phase transformation mechanisms responsible for microstructural evolution in welds.

Contact: John W. Elmer, Lawrence Livermore National Laboratory
Phone: (925) 422-6543, Fax: (925) 423-7040, E-mail: elmer1@llnl.gov



Real time 3-dimensional simulation of grain size evolution in the HAZ of a 1.9 kW GTA weld moving at 1.1 mm/s in titanium. Fluid flow vectors are shown in the liquid weld pool (red) for the weld that is moving from left to the right.

Molecularly Directed Mixing in Polymer Composite Processing

J. Liu, G. J. Exarhos, and W. D. Samuels, Pacific Northwest National Laboratory

E. S. Peterson, Idaho National Engineering and Environmental Laboratory

B. I. Lee and Z. Cao, Clemson University

Motivation—Both improved fracture strength and thermal stability are expected upon combining a polymer precursor with another material to form a composite. However, poor mixing of the constituents and inattention to the attendant interfacial interactions, can actually degrade strength and stability of the resulting material. Two approaches to enhance intimate mixing and control of interfacial interactions are based upon the use of a surfactant to promote dispersion of one phase within the other, or the use of chemical routes to induce molecular scale mixing during precursor condensation to form a true molecular composite. While the use of nonionic surfactants to stabilize ceramic powder dispersions is well known, their efficacy at dispersing carbon nanotubes in a polymer matrix has not been shown. Recent Center associated research demonstrates for the first time marked improvement in physical properties of polymer composites containing a well-dispersed carbon nanotube phase. Related activities also demonstrate significant property improvement in polymer/ceramic composites when intimate mixing of precursors is forced to occur on the molecular level.

Accomplishment—A stable dispersion of multi-walled carbon nanotubes in acetone was achieved through the use of polyethylene oxide-8-lauryl. To this mixture was added bisphenol-A epoxy resin and a hardener. This well-stirred solution was cast and cured. Contrasting morphologies of the resulting polymer composites both containing and devoid of the surfactant are shown in Figure 1. In addition to a significantly higher degree of homogeneity, the polymer composite prepared with surfactant

showed an increase in glass transition temperature from 63°C to 88°C and an increase in elastic modulus of over 30% when compared with the composite prepared without the surfactant.

In related work that also demonstrates the influence of mixing on attendant properties, the sol-gel processing route was used to synthesize a molecularly mixed inorganic polymer composite. Silicophosphate sols were prepared by combining phosphorus pentoxide directly with a liquid silicon alkoxide to form a crosslinked network, followed by subsequent heating at 100°C. Remarkably, silicon in a hexavalent coordination state was seen in the solid state ^{29}Si NMR spectrum (Figure 2). This bonding geometry usually only exists at high temperatures or in samples synthesized at exceedingly high pressures.

Significance—Surfactant directed dispersion of carbon nanotubes in polymer composite materials markedly improves mechanical strength and thermal stability of the composite allowing use under conditions where the material ordinarily would fail. The improved materials strength would also contribute to a weight reduction that would promote vehicle efficiency and render such materials suitable for aircraft applications. Mixing of composite precursor materials at the molecular level can also lead to modification of localized chemical bonding observed only when a material is processed under much more severe and energy intensive conditions. In the case of silicon, 6-fold bonding is expected to enhance the mechanical strength of a material as well as its catalytic activity.



Figure 1a. SEM micrograph of a carbon nanotube/epoxy composite prepared without surfactant addition. The multiwall carbon nanotubes average 30 nm in diameter and are poorly dispersed in the matrix.

Figure 1b. SEM micrograph of the carbon nanotube/epoxy composite prepared with surfactant showing uniform dispersion of one phase within the other.

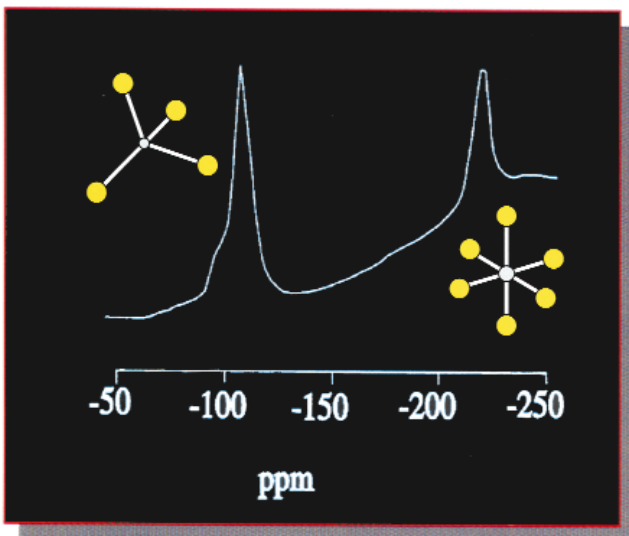


Figure 2. ^{29}Si NMR spectrum of a molecularly mixed silicophosphate molecular composite. The presence of hexavalent silicon is indicated by the resonance feature near 213 ppm.

Engineered Transport Properties in Polymeric Membranes

J. McBreen, Brookhaven National Laboratory

E. S. Peterson, Idaho National Engineering and Environmental Laboratory

J. Liu, G. J. Exarhos, W. D. Samuels, Pacific Northwest National Laboratory

Motivation—Polymer membranes find extensive use in applications ranging from ion-conducting electrolytes for advanced high capacity batteries to ion sieves for remediation of waste streams. For lithium battery applications, both a high ionic conductivity and a high lithium ion transference number are critical to performance, while improved ion sieves demand selective ion retention capability as well as an enhanced ion retention capacity that scales with surface area. For both applications, chemical robustness of the membrane is mandatory. These requirements can be engineered into polymer membranes through chemical modification of the membrane and its pore structure during processing.

Accomplishment—Inorganic polymer membranes based upon polysiloxanes, $-\text{[R}_2\text{Si-O]}_x-$ or the isoelectronic polyphosphazenes, $-\text{[R}_2\text{P=N]}_x-$, comprise the matrix materials for ongoing investigations. Two approaches have been pursued to address the ion transport problem in these materials. A new family of anion acceptors based upon electron deficient boron sites on borane or borate compounds containing various fluoridated aryl or alkyl groups has been synthesized (Figure 1). These acceptors, upon grafting to a polymer backbone, promote the dissolution of normally insoluble salts such as LiF in non-aqueous solvents thereby increasing charge carrier concentrations. Several of these materials have been tested in the corrosive environment of rechargeable Li/LiMn₂O₄ batteries and found to

improve battery performance in addition to promoting enhanced materials stability. An alternate approach to improve battery performance focuses upon modification of the network structure of the polymer through formation of a molecular composite with silica. (Figure 2) Phosphazene/silica composite membranes, prepared by a hydrolysis-condensation process, provide dimensional stability, induce flexibility (low glass transition temperature), and improve ion conductivity.

Significance—Electrolyte stability during charge/discharge cycles is of critical importance for improving the performance of alkali metal based batteries. The highly reactive chemical environment inherent to such systems readily can degrade many prospective polymer electrolyte systems rendering them unsuitable for such applications. In addition to electrolyte durability, high cationic conductivity is required which mandates equivalency of the cation and anion transference numbers in order to suppress polarization effects that eventually can degrade the ionomer. For vehicle applications, battery operation over a wide temperature range from at least -40°C to $+120^\circ\text{C}$ is a principal requirement. The thermal requirement imposes yet another constraint on the performance characteristics of the polymer electrolyte. Development of an advanced polymer electrolyte for lithium batteries demands engineering of new materials that can meet these rather stringent operating requirements.

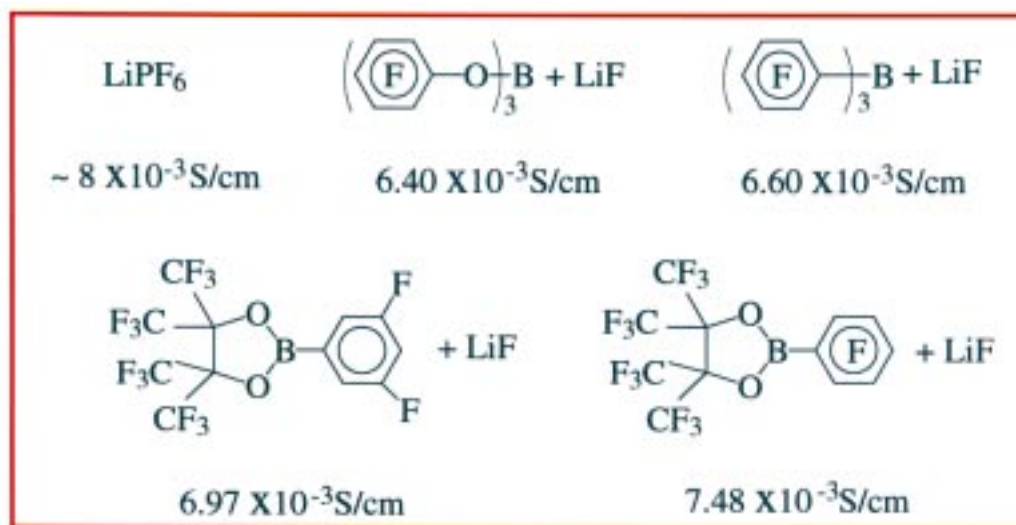


Figure 1. Boron-containing anion acceptors and related lithium ion conductivities in equimolar mixtures of LiF in DME. When grafted to a polymer matrix, these chemical groups promote charge carrier dissolution and enhanced conductivity.

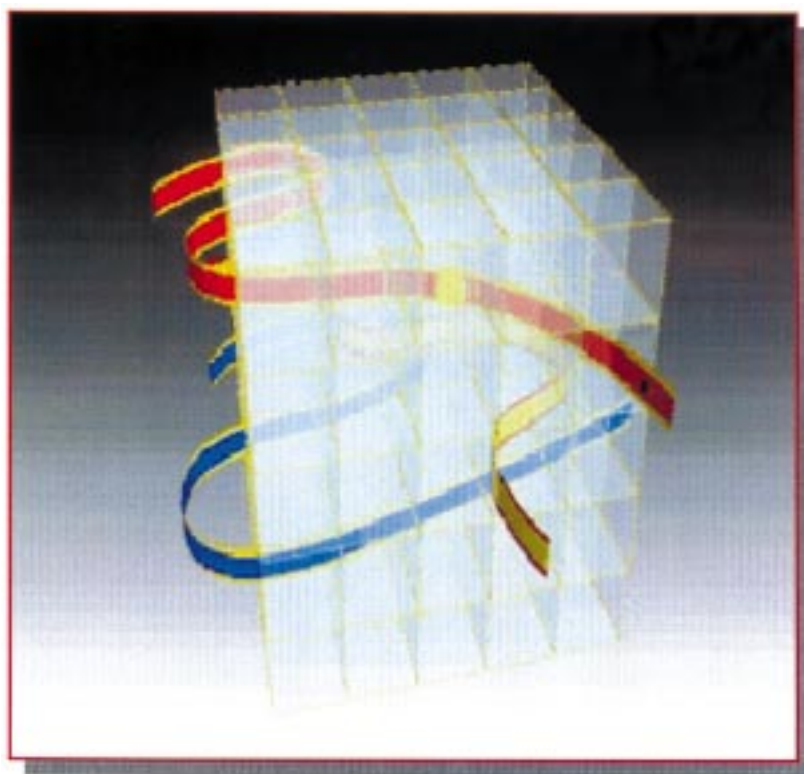


Figure 2. Illustration depicting permeation of a polymer electrolyte through a polymer/ceramic nanomolecular composite. The interconnected nanoarchitecture promotes conductivity while enhancing the chemical robustness of the composite.

Anisotropic Conductivity in Molecular Wires

E. S. Peterson, Idaho National Engineering and Environmental Laboratory

Motivation—Certain transition metal complexes form linear chain arrangements in which the d_z electron orbitals of the metal atoms overlap, allowing extended electron delocalization in one dimension. Such "linear polymers" exhibit electronic conductivity along that direction where the magnitude of the conductivity is controlled by the degree of d_z orbital overlap. To design materials with increased electron flow along the chain, the chemical and structural factors that influence this overlap must be understood. The nature of the ligand bound to the metal center, the degree of oxidation of the molecular chain, and the presence of surrogate charge compensating cations are all thought to influence this conductivity. Center related work strives to understand the influence of these parameters on molecular structure and the attendant conductivity.

Accomplishment—An electrolytic method has been developed for synthesis of model platinum compounds which exhibit one dimensional electronic conductivity. The chain structure of the well-known potassium tetracyanoplatinate(II) material, $K_2Pt(CN)_4$, is shown in Figure 1 along with an STM image. Mild oxidation induces the

conductivity. By replacing the cyanide groups with bidentate oxalate ligands, the bis-platinum(II) oxalato complex can be formed and is shown in Figure 2. STM images of this complex, also shown in the figure, exhibit cooperative growth and marked interchain interactions. Synthesis conditions for these linear polymeric chains can be controlled so as to influence their propagation direction. Continuous polymer chain bundles with lengths approaching 30 cm and cross-sections less than 0.5 mm in diameter have been prepared.

Significance—All of these materials show excellent potential for application in the field of microelectronics due to their highly anisotropic conductance properties arising from the overlap of the d_z platinum electron orbitals. Since processing methods have been developed to promote linear chain growth, electrical connectivity between two points can likely be achieved. It also is expected that the conductivity anisotropy will be accompanied by an anisotropic optical response related to directional free carrier absorption along a preferred direction in the material.

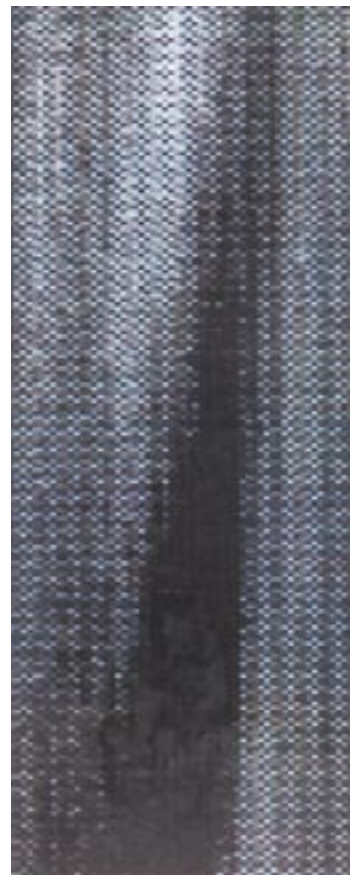
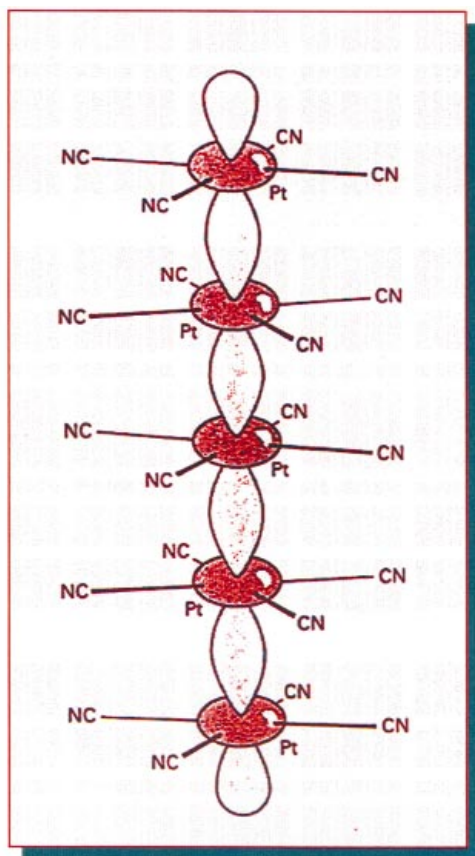


Figure 1. Representation of the linear chain-like molecular structure of the tetracyano platinum (II) anion showing the d_z orbital overlap (top). An STM image of the slightly oxidized form of this material overlaid with the inferred atomic positions appears to the right.

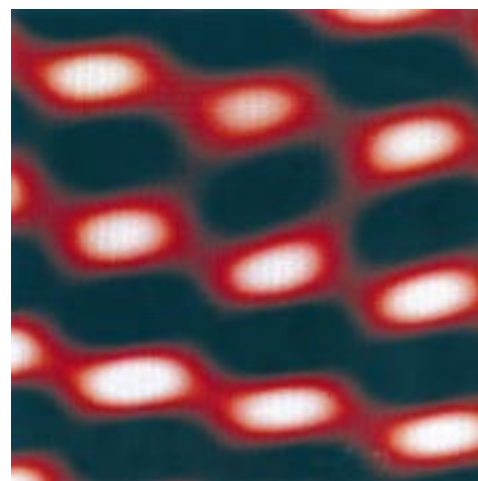
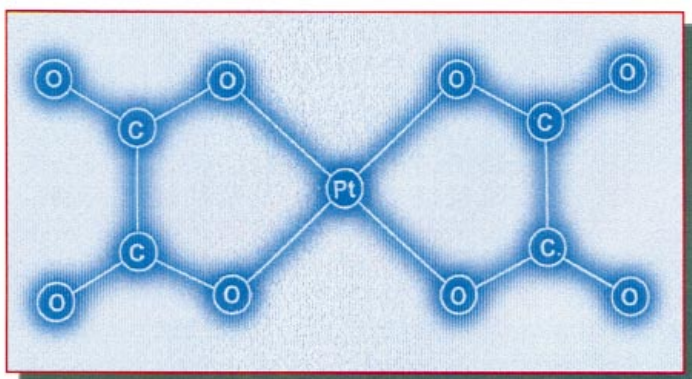


Figure 2. Molecular structure of the bis-oxalato platinum (II) anion (top). An STM image of potassium bis-oxalato platinate (II) is shown to the right. The image depicts both the planar $[\text{Pt}(\text{ox})_2]^{-2}$ anion and illustrates the interchain ligand/ligand interaction.

Improved Microstructural Control of Melt-Spun Nd₂Fe₁₄B

*L. H. Lewis, Brookhaven National Laboratory
M. J. Kramer and R. W. McCallum, Ames Laboratory*

Motivation—The technical magnetic properties of advanced permanent magnetic materials are dominated by the scale, alignment and homogeneity of the microstructure. These materials characteristics are very difficult to control during processing, especially in permanent magnetic materials fabricated by rapid solidification techniques which have the potential to produce a nanostructured material with a high energy product and significant corrosion resistance. Thus, there exists significant drive to exert more control over the microstructural development in rapidly-solidified advanced permanent magnetic materials, facilitating the development of higher energy product magnetic materials for use in motors, actuators and sensors.

Accomplishment—Systematic synthesis and investigation of stoichiometric melt-spun Nd₂Fe₁₄B have revealed the overriding importance of the atmospheric conditions during rapid solidification. Figure 1 provides a view of the melt-spinning process, in which a molten stream of material is injected onto a rapidly-rotating water-cooled Cu wheel. Depending upon the tangential speed of the Cu wheel, the nominal microstructure of metallic melt-quenched products may range from x-ray amorphous (over-quenched) to microcrystalline (under-quenched) as the latent heat of fusion is removed from the molten stream.

The melt-spinning process is carried out in a controlled atmosphere, necessary to avoid catastrophic oxidation of the melt-spun materials. However, it is apparent that the atmosphere also controls the rate of progression of the solidification front as it moves from the wheel-liquid contact area through the thickness of the ribbon.

This effect is illustrated in Figure 2, which displays magnetic force microscopy images of magnetic domain configurations in samples of Nd₂Fe₁₄B ribbon, melt-spun at 10 m/sec in three different atmospheric conditions: Ar (750 Torr), He (750 Torr or 250 Torr). The cross-sectional microstructure is highly non-uniform in samples quenched in a large pressure of Ar or He, revealing a discontinuous magnetic domain scale which reflects the abrupt change in grain size produced by recalescence as the solidification front consumes the ribbon. In contrast, the material quenched at the lower He pressure is homogeneous and nanoscaled, with few macro-crystalline regions. This trend is echoed in the micrographs of Figure 3, which display plan-views of the wheel surface of the ribbons. The ribbon quenched at low pressure replicates the polished surface of the Cu wheel and is free from the trapped gas bubbles visible on the ribbons quenched at higher gas pressures.

Significance—It is recognized that the pressure and type of gas utilized during the rapid solidification process determines the overall quench rate of the Nd₂Fe₁₄B liquid which, in turn, delineates the resultant ribbon microstructure. The observed differences in the microstructure of the Nd₂Fe₁₄B melt-quenched ribbons may be attributed to the differences in heat capacity of the gases utilized during melt-spinning as well as the contiguity of the melt-stream/Cu wheel contact. These developments may allow the fabrication of highly uniform overquenched materials that may be briefly annealed to produce a material with a fine-scale, homogeneous microstructure and optimized magnetic properties.

Contact: Laura H. Lewis, Brookhaven National Laboratory
Phone: (631) 344-2861, Fax: (631) 344-4071, E-mail: lhlewis@bnl.gov

Figure 1. The melt spinner.

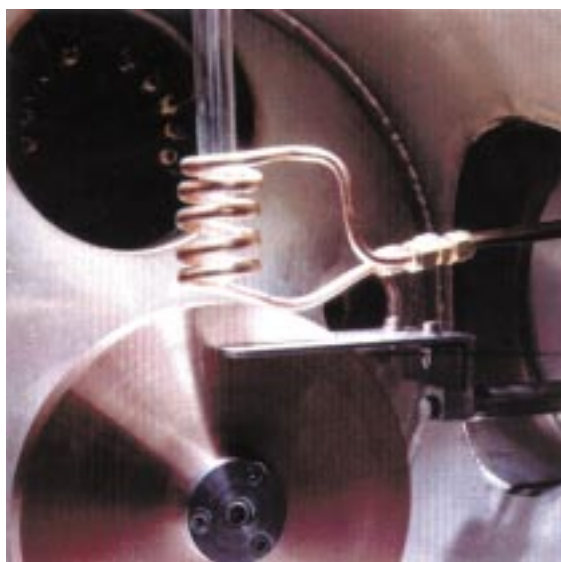


Figure 2. Cross sectional view of magnetic domain structure of quenched $\text{Nd}_2\text{Fe}_{14}\text{B}$ ribbons.

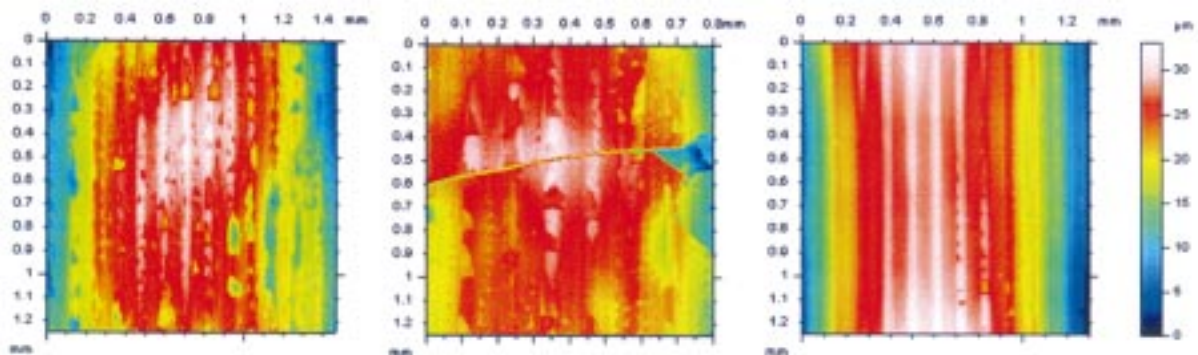


Figure 3. Plan-view of ribbons, wheel side surface. Low pressure replicates wheel surface.

Nanocomposite Pr-Co Magnets

*D. J. Branagan, Idaho National Engineering and Environmental Laboratory
M. J. Kramer, Yali Tang, and R. W. McCallum, Ames Laboratory*

Motivation—Permanent magnetic materials are a cornerstone of many modern technologies and serve as key components in many industrial and consumer devices. To perform useful work, a magnet must be made 'permanent', i.e., it must trap a high density of magnetic energy in metastable states. This requires high energy barriers that prevent the magnet from reverting to its unmagnetized ground state. Careful control of both the composition and the processing conditions is required in order to develop appropriate microstructures capable of storing high energy densities. While permanent magnets based on SmCo_5 are technologically important, magnets made from the isostructural PrCo_5 phase have never been commercially developed even though the Pr compound has very favorable intrinsic magnetic properties. Developing microstructures with the ability to store high energy densities in the Pr-Co system has been difficult due to unfavorable phase equilibria and the metastability of the PrCo_5 phase which spinodally decomposes below 850°C . By developing optimum microstructures which exhibit single phase magnetic character, the energy density of the Pr-Co magnet could be improved dramatically potentially allowing commercial exploitation of this material.

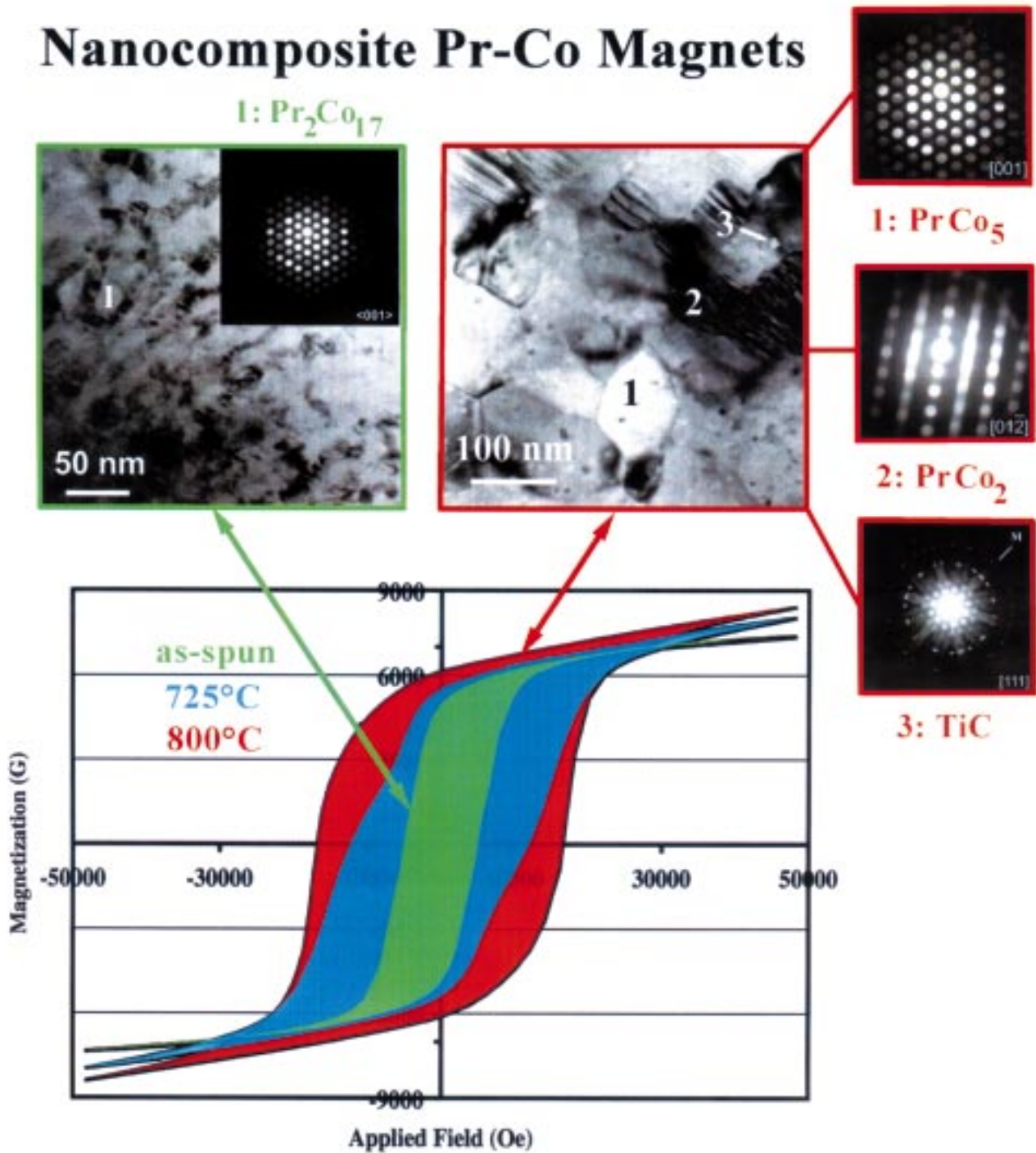
Accomplishment—Consistent with previous results, it was found that it was not possible to avoid the formation of deleterious Pr rich soft ferromagnetic phases in the binary Pr-Co system during solidification. However, these unwanted phases could be avoided in a quaternary Pr-Co-Ti-C alloy containing greater than 6 at% carbon since the alloy resides in a favorable three phase system containing only one ferromagnetic phase. The excess Pr over the PrCo_5 stoichiom-

etry formed the PrCo_2 phase which is paramagnetic at room temperature. Carbon chemically stabilized the PrCo_5 phase preventing spinodal decomposition. The extra carbon necessary to alter the phase equilibria was removed from solid solution by TiC precipitation forming a grain stabilized nanoscale composite structure. After heat treating at 800°C , an extremely fine magnetically favorable microstructure was developed which consisted of 75-100 nm PrCo_5 hard magnetic grains, 75-100 nm PrCo_2 second phases, and < 10 nm TiC grain boundary precipitates. The achievement of hysteresis loops exhibiting single phase magnetic character resulted in high values of energy product which represented 90% of the theoretical isotropic maximum (Fig. 1).

Significance—Current and expanding applications for rare earth magnets include devices such as small motors in cars, starter motors, air bag sensors, hybrid generators, transmission solenoids, DC power tools, etc. Since each of these applications has different requirements, no single magnet material is expected to meet all needs. While Nd-Fe-B type magnets are the strongest and are used in a wide variety of applications, this material is limited to near room temperature applications due to its low Curie temperature (583 K). This creates problems for applications at elevated temperature (> 400 K). Thus, there continues to be significant interest in rare earth cobalt type permanent magnets due to their extremely high Curie temperatures. The PrCo_5 phase has a Curie temperature which is over 400 degrees greater than Nd-Fe-B and may allow significant improvements in magnet performance at elevated temperatures.

Contact: Daniel James Branagan, Idaho National Engineering and Environmental Laboratory
Phone: (208) 526-4674, Fax: (208) 526-0690, E-mail: brandj@inel.gov

Nanocomposite Pr-Co Magnets



Shown are hysteresis curves and the corresponding TEM micrographs and selected area diffraction patterns identifying the phases for the as-spun and heat treated (at 725°C and 800°C) quaternary Pr-Co alloys.

Modeling High-Performance Magnets

J. S. Jiang, E. E. Fullerton, and S. D. Bader, Argonne National Laboratory

Motivation—A promising new pathway to achieve permanent magnets with high energy-products lies in the nano-assembly of known hard and soft magnetic phases that are exchange coupled at the interfaces. This approach stands in stark contrast to previous attempts that enlist blind Edisonian searches for new materials that have desired hard magnetic properties. Recently, nano-crystalline "exchange-spring" magnets have been produced by bulk processing methods such as melt-spinning and mechanical alloying. The present work complements those efforts and provides a thin-film approach that overcomes the random nature of such composite materials. The full potential of exchange hardening can thusly be realized, and the optimization of the hard-magnet properties is no longer a "trial-and-error" process.

Accomplishment—Thin films can be used to design a model materials system where virtually all aspects of the exchange spring-coupling phenomenon can be systematically controlled and examined. This has allowed for direct comparison with a theoretical model and provides a more realistic prediction of achievable energy product in exchange-spring magnets.

Using a buffered epitaxial growth method, SmCo alloy films have been successfully synthesized by sputter deposition with room-temperature coercivity values as large as 3.4 Tesla. The anisotropy properties of these hard SmCo films were found to correlate closely with their microstructural characteristics. Exchange spring bilayer and superlattice structures were

synthesized with SmCo layers as the hard phase and with Fe or Co layers as the soft phase (Fig. 1). The demagnetization of the soft layers is fully reversible as expected for an exchange-spring magnet. The maximum energy product $(BH)_{\max}$ is increased from ~ 11 MGOe for a single SmCo film to ~ 14 MGOe for a superlattice composed of 100-Å Co and 450-Å SmCo layers. A micromagnetic model which utilizes anisotropy and exchange constants characteristic of the individual layers was developed to describe the magnetization reversal process and to provide detailed information on the energetics of magnetic domain-walls in the hard and soft layers. Model calculations of the dependence of $(BH)_{\max}$ on the layer thicknesses indicate that the fundamental length scale for exchange spring magnets is the domain wall thickness, and that very large values of energy product are attainable in exchange-spring structures with suitably chosen constituent components (Fig. 2).

Significance—High-performance permanent magnets may afford the advantages of increased efficiency in energy production and energy systems. The highlighted work is aimed foremost to explore the basic properties of new interfacial materials. This well-characterized model system permits the testing of modern micromagnetic theories, and the investigation of its magnetic properties can greatly aid the development of more complex nanostructures and the quest to synthesize high-performance, exchange-spring permanent magnets.

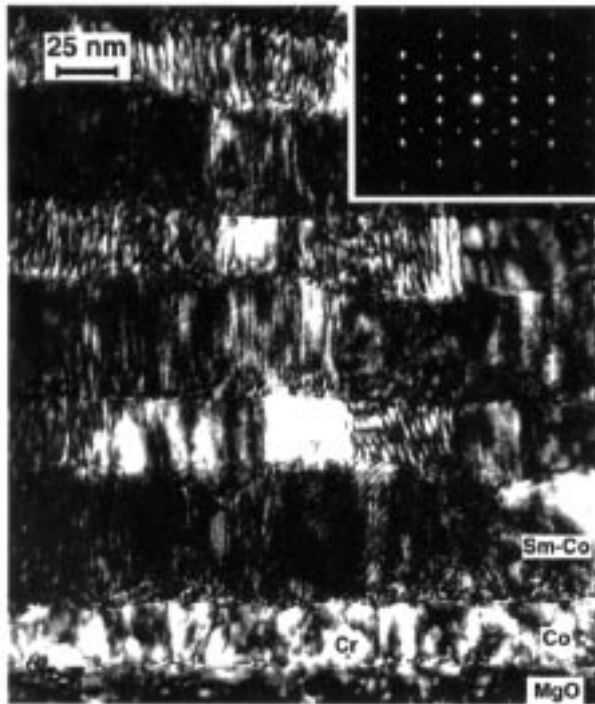


Figure 1. Dark-field cross-sectional TEM micrographs and the electron diffraction pattern of a Sm-Co/Co superlattice.

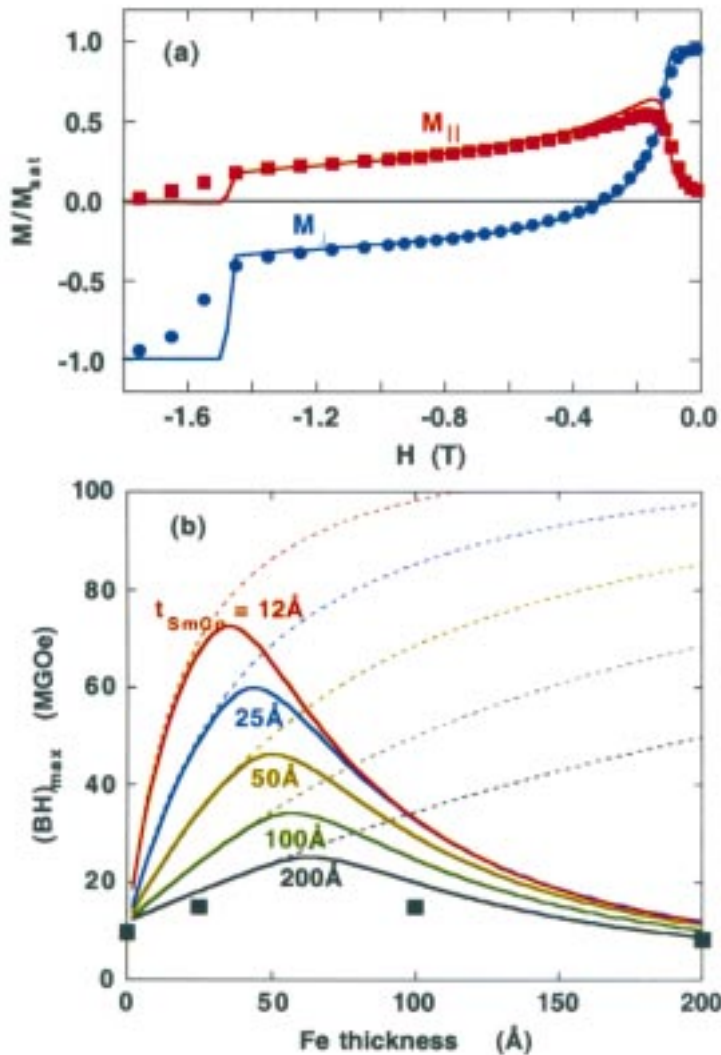


Figure 2. (a) Measured demagnetization curves (squares: longitudinal component $M_{||}$; circles: transverse component M_{\perp}) of a Sm-Co/Fe(200 Å) bilayer structure. The solid curves are results of numerical calculations using the intrinsic parameters of the individual layers. (b) Calculated maximum energy product $(BH)_{max}$ of Sm-Co/Fe bilayers with different layer thickness. The dashed curves are for the ideal $(BH)_{max} = (2\pi M)^2$. The theoretical $(BH)_{max}$ of Nd-Fe-B is 64 MGOe and typical values for commercial material are <50 MGOe.

Three-Dimensional Modeling of Nanoindentation

*J. A. Knapp, D. M. Follstaedt, S. M. Myers, G. A. Petersen and J. C. Barbour,
Sandia National Laboratories, New Mexico*

Motivation—In developing hard surface layers for softer substrates, it is also necessary to develop methods that accurately quantify the mechanical properties of these thin layers. For this purpose, we combined ultra-low load indentation to sub-micrometer depths within the layer ("nanoindentation") with finite-element modeling of the indenter force required as a function of depth. Modeling the combined material response of the layer and substrate is necessary because the softer substrate is compressed even at shallow depths, and thus influences the apparent properties of the layer. With modeling, the layer properties can be quantified independently of the substrate. Our work has relied upon 2-D, axisymmetric models with cylindrical symmetry about the indentation axis, ignoring possible effects of the three-sided indenter geometry. This approach has been successfully applied to hard layers of interest in the Center, including ion-implanted metals, ceramic deposited layers, and very hard diamond-like carbon layers. The results appear accurate after many internal consistency checks.

Accomplishment—In parallel with the above work, we have been developing 3-D finite-element modeling of nanoindentation that takes account of the actual indenter shape. These more difficult calculations allow us to verify the accuracy of 2-D calculations and extend our understanding of nanoindentation to more challenging material problems. In Fig. 1, the indenter force versus depth curves are compared for 2-D and 3-D calculations. Both calculations (using the ABAQUS 5.8 code) modeled deformations in Si with a mesh whose radius and depth were 5 μm , and used the same mechanical properties (yield strength = 5.18 GPa; Young's modulus = 175.2 GPa) to allow direct compari-

son between the results; in this example, the diamond indenter was modeled as perfectly rigid. Good agreement between the two methods is obtained, with the 3-D calculation predicting only slightly higher ($\sim 3\%$) force at 150 nm depth. Figure 2 shows the mesh used to divide Si into small elements, and the residual deformation (110 nm depth) and Mises stress in the material after withdrawal of the indenter. The edge of the 60° sector with higher residual stress (red areas) corresponds to the sharp corner of the indenter tip, where greater deformations are expected. The vertical and radial dimensions of the Si elements are similar to those of 2-D models, but the lateral dimensions of elements near the corner had to be made sufficiently fine to account for lateral material flow and to achieve convergence in the calculation. We plan to compare such predicted residual deformations to residual impressions measured on indented Si by surface microscopy.

Significance—The agreement in Fig. 1 and similar tests with metals confirm the accuracy of 2-D calculations for predicting force versus depth during indentation. Since the 2-D calculations run much faster than 3-D ones (20 min. versus 60 hr. on a 450 MHz workstation), we use the former for our routine materials analyses. In addition, with recent improvements to the modeling, our 3-D calculations are now robust enough to be used regularly to provide additional insight into the properties of materials undergoing nanoindentation testing. For instance, Fig. 2 indicates that the stresses vary by more than 10x in the azimuthal direction, and thus 3-D calculations appear important for understanding the stresses leading to cracking of some materials at the indenter corners.

Contact: James A. Knapp, Sandia National Laboratories, NM
Phone: (505) 844-2305, Fax: (505) 844-7775, E-mail: jaknapp@sandia.gov

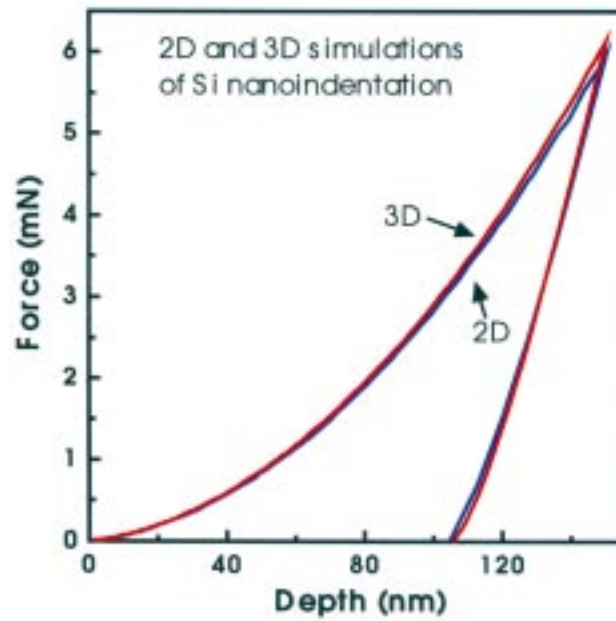


Figure 1. Nanoindentation force vs. depth calculated using a 2-dimensional axisymmetric mesh compared to a calculation using a 3-dimensional mesh. Both meshes were 5 μm in radius and depth. The two calculations modeled the indenter tip as rigid and having the same cross-section area as a function of vertical position.

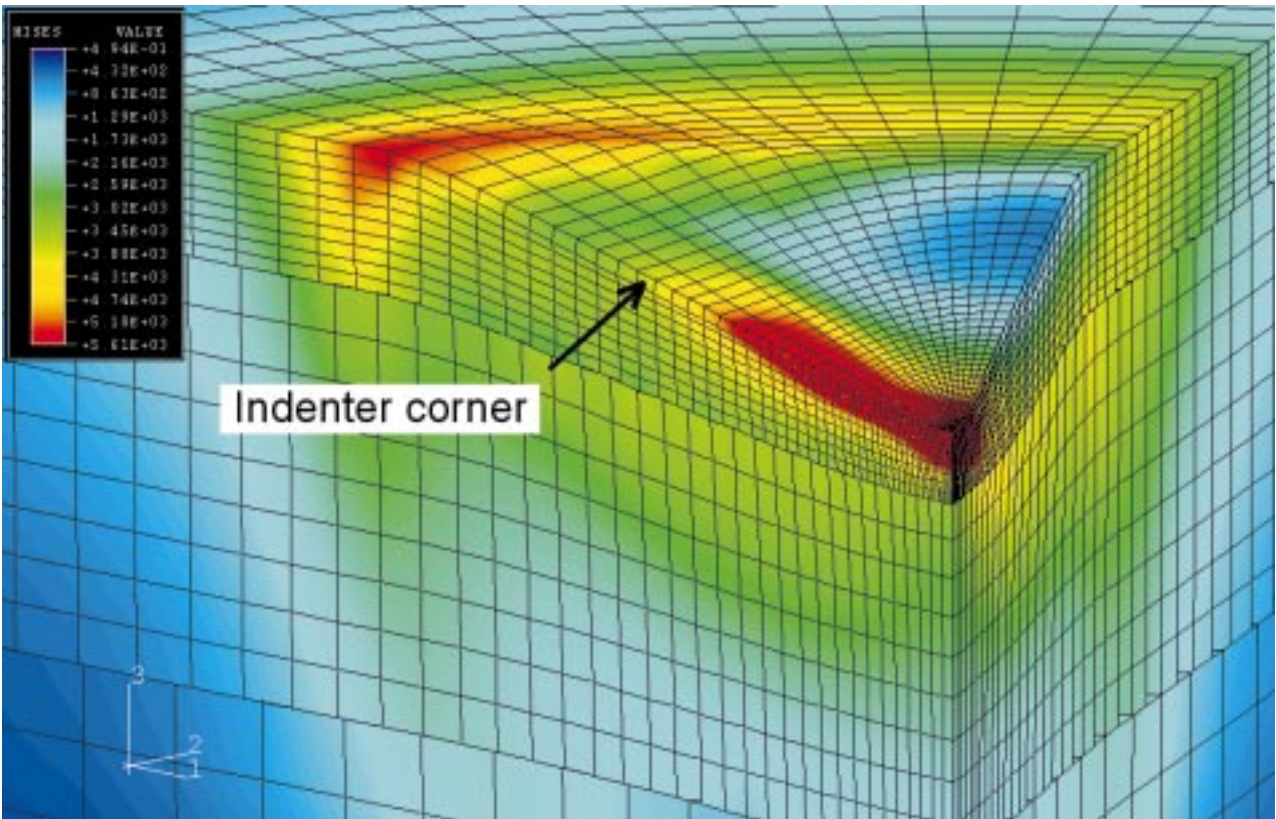


Figure 2. Three-dimensional mesh after indentation, showing surface deformation and residual stress. Because of the symmetry of the pyramid-shaped indenter, it is only necessary to model a 60° pie-shaped sector of the sample and indenter.

Ultrananocrystalline Diamond Thin Films

*Dieter M. Gruen, Alan R. Krauss, Ali Erdemir, and Anirudha V. Sumant,
Argonne National Laboratory*

Motivation—Diamond is the hardest material and also has a very low coefficient of friction. This combination of desirable characteristics provided much of the impetus for the tremendous research activity engendered by the discovery of CVD methods for diamond film synthesis some twenty years ago. However, the methods developed at that time relied on the use of hydrocarbon-hydrogen gas chemistries. These methods largely produced coatings that have a high surface roughness mirroring the film microstructure, which is typically composed of micron-sized crystallites. The use of such films in tribological applications has, therefore, been quite limited. It became apparent that CVD methodologies had to be developed that would lead to films of very low surface roughness in order to be useful in sliding seal applications, for example.

Accomplishment—We have explored the role of atomic hydrogen in diamond CVD and discovered that regasification of embryonic diamond nuclei drastically lowers secondary heterogeneous nucleation rates, thus allowing only the largest crystallites to survive the growth process. Successive replacement of hydrogen by argon in microwave plasmas containing small amounts of carbon containing molecules

revealed a new compositional domain at high argon content where secondary nucleation rates are of order $10^{10} \text{ cm}^{-2} \text{ sec}^{-1}$. In this regime, the diamond microstructure consists of 3-5 nm crystallites. The phase-pure nanocrystalline diamond films produced in this way have been extensively characterized both experimentally and theoretically (e.g., molecular dynamics, density functional, and tight-binding calculations). The films are very smooth (20-30 nm rms) and maintain their nanocrystallinity even at thicknesses exceeding 30 μm . The grain boundary carbon is largely p-bonded; and since approximately 10% of the total carbon is at the grain boundaries, the mechanical, electrical, and optical properties are profoundly affected.

Significance—These smooth thin diamond films have great promise for many technological applications. As a first step, SiC rotary shaft pump seals have been coated to a thickness of 2 μm with nanocrystalline diamond films, and their performance relative to uncoated seals has been evaluated in a liquid pumping system operating at 3600 rpm and 100 psi water pressure. The results of the tests, shown in Figs. 1 and 2, reveal remarkable performance.

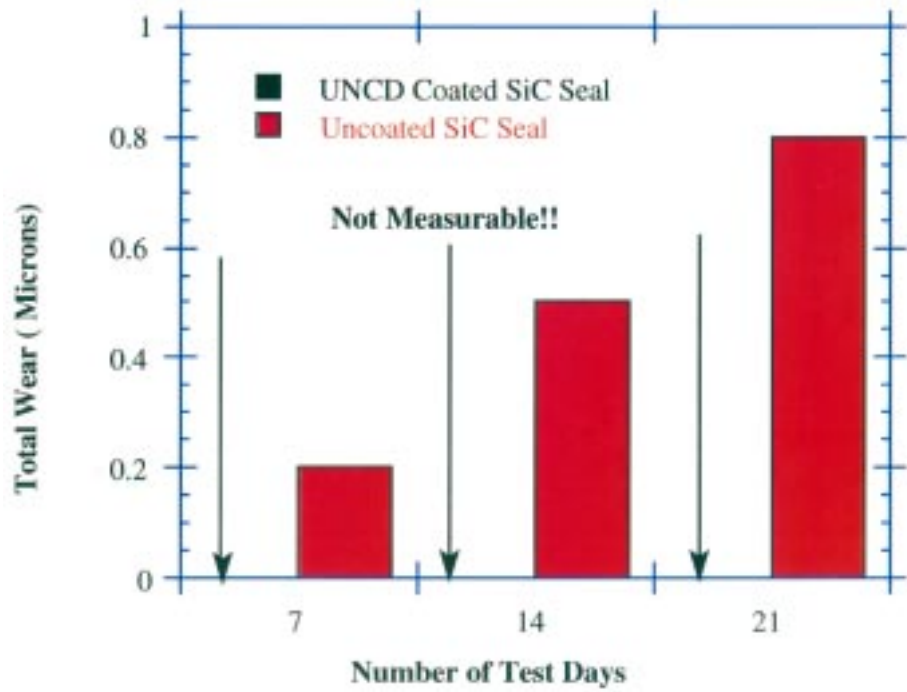


Figure 1. Comparison of Wear on UNCD Coated and Uncoated SiC Seal (After 21 days Test).

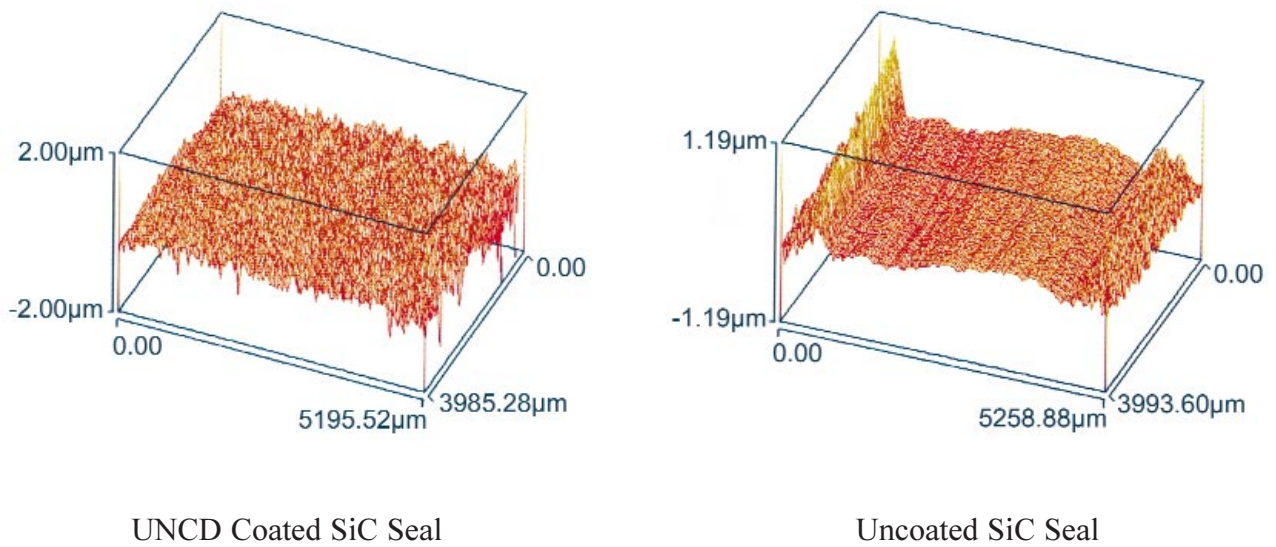


Figure 2. 3D profile of Wear Tracks on UNCD Coated and Uncoated SiC Seal (After 21 days Test).

Oxide Defects and Damage Processes in Protective Alumina Films

*P. F. Tortorelli, B. A. Pint, E. A. Kenik, K. L. More, and I. G. Wright,
Oak Ridge National Laboratory*

Motivation—Thermally grown oxide scales can provide high-temperature oxidation protection if they are slow-growing, sound, and adherent to the substrate. Consequently, the nature of the defects and damage processes in such oxides has been the subject of fairly extensive study over the past ten years and a number of mechanical, and chemical scale failure models have been proposed based on various analytical considerations and/or empirical observations. Yet, there is still much uncertainty about the mechanisms leading to film decohesion, particularly as related to prediction of the time to loss of oxide protection by film spallation as a function of substrate composition and strength and the nature of imposed stresses. This study was thus designed to evaluate a deterministic role of alumina defects/damage on film spallation.

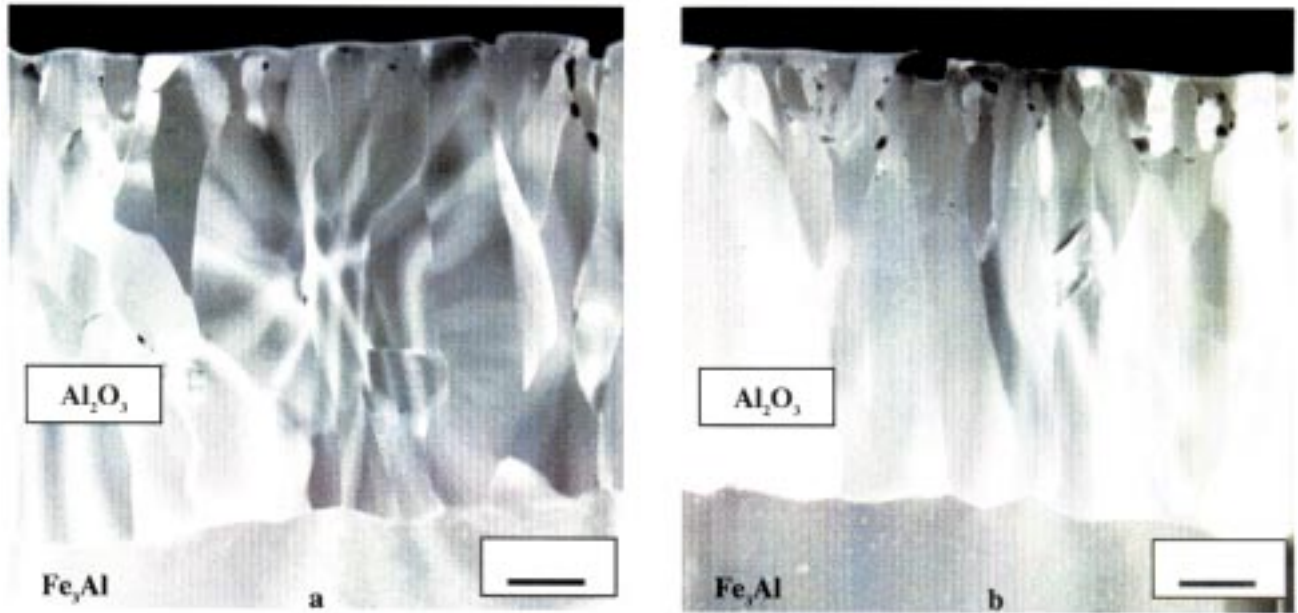
Accomplishment—This study utilized an experimental approach based on a microstructural comparison of isothermally and cyclically oxidized specimens exposed for the same time and temperature. Oxidation conditions were chosen so that exposures were terminated prior to the onset of general oxide film spallation. In this way, possible differences in incipient scale damage were investigated and conclusions about the relevance of defects to film spallation can be made. Optical imaging and scanning and scanning transmission electron microscopy were used to compare oxide-metal cross sections from specimens of Fe-Al, FeCrAlY, and NiCrAlY alloys that were thermally cycled to those that were isothermally exposed. In every case, thermal cycling ultimately led to greater oxide film spallation compared to isothermal exposures. However, oxide characterization across this wide range of imaging magnification did not indicate any significant microstructural differences between isothermally and cyclically oxidized specimens

for any of these alumina-forming alloys. The major defect type found in all of the films was porosity predominately located nearer the oxide-gas interface. However, this type of porosity was observed under both isothermal and cyclic oxidation exposures and therefore could not be related to the observed differences in film spallation behavior. Indeed, there was no microstructural evidence for differences in defect production or accumulation between the two oxidation protocols.

Significance—Some important implications regarding the relationship of oxide defects and their development to film spallation and failure can be made based on the fact that the relatively straightforward comparative approach used in this work failed to reveal evidence of incipient defects or damage in three different alumina-alloy systems. These findings can be interpreted as indicating that fundamental processes controlling oxide growth and adherence do not necessarily manifest themselves in terms of damage accumulation. For example, for oxide spallation by adhesive failure, changes in interfacial energies/properties can ultimately control failure without extensive defect production. In such cases, overall strain energy considerations can well be paramount. The results of this study obviously call into question models in which defect production and damage development determine the nature of oxide spallation and the loss of oxidation resistance. The present observations would indicate that there are cases where the factors controlling the proclivity to film spallation and failure are set well before significant oxide and interfacial damage has accumulated.

Research sponsored by the Division of Materials Sciences, Office of Science and the Office of Industrial Technologies, U. S. Department of Energy.

Contact: Peter Tortorelli, Oak Ridge National Laboratory
Phone: (865) 574-5119, Fax: (865) 241-0215, E-mail: tortorellipf@ornl.gov



Scanning transmission electron images of Al₂O₃ grown on Fe₃Al at 1200°C using (a) 20-h isothermal exposure or (b) 20 1-h cycles. There were no microstructural differences in defect or interfacial structures between the two cases (at any length scale) despite significantly greater susceptibility for oxide film spallation at longer times for the case represented by (b). Oxide-metal cross sections were prepared by focused ion beam milling thereby enabling imaging of full oxide thickness.

Sulfur Segregation to Dynamic Al₂O₃-Metal Interfaces

P. Y. Hou, Lawrence Berkeley National Laboratory

Motivation—It is well known that impurities and/or solutes in an alloy can segregate to the free surface and to the alloy grain boundaries at elevated temperatures. When a metal or alloy undergoes oxidation, an external oxide film is formed from the transport of metal outward and of oxygen inward. It has been proposed that sulfur, which is a common impurity in alloys, segregates to the growing oxide-metal interface and weakens the interfacial bonds as it does when present at alloy grain boundaries. However, it is not well established if sulfur should segregate to an intact interface, where the oxide remains adherent to the underlying alloy. Rather, the detection of sulfur at oxide-metal interfaces after thermal treatment has been often attributed to segregation after scale detachment due to the thermal stresses present during cooling, or from accumulation as a result of oxide growth, where the interface advances inward. The purpose of this work is to examine the time dependence of the concentrations of sulfur and other impurities at growing oxide film/alloy interfaces to better understand the dynamic segregation phenomena associated with high-temperature oxidation and the adherence of the protective surface oxide.

Accomplishment—The amount of sulfur segregated to the growing Al₂O₃/alloy interface as a function of time was studied using Auger electron spectroscopy after the oxide film was debonded by scratching using a Vickers micro-indenter in ultra high vacuum. Oxide films grown on two alumina-forming alloys were studied. One was Fe₃Al (Fe-28Al-5Cr, at.%) and the other alloy was Fe-18Cr-10Al.

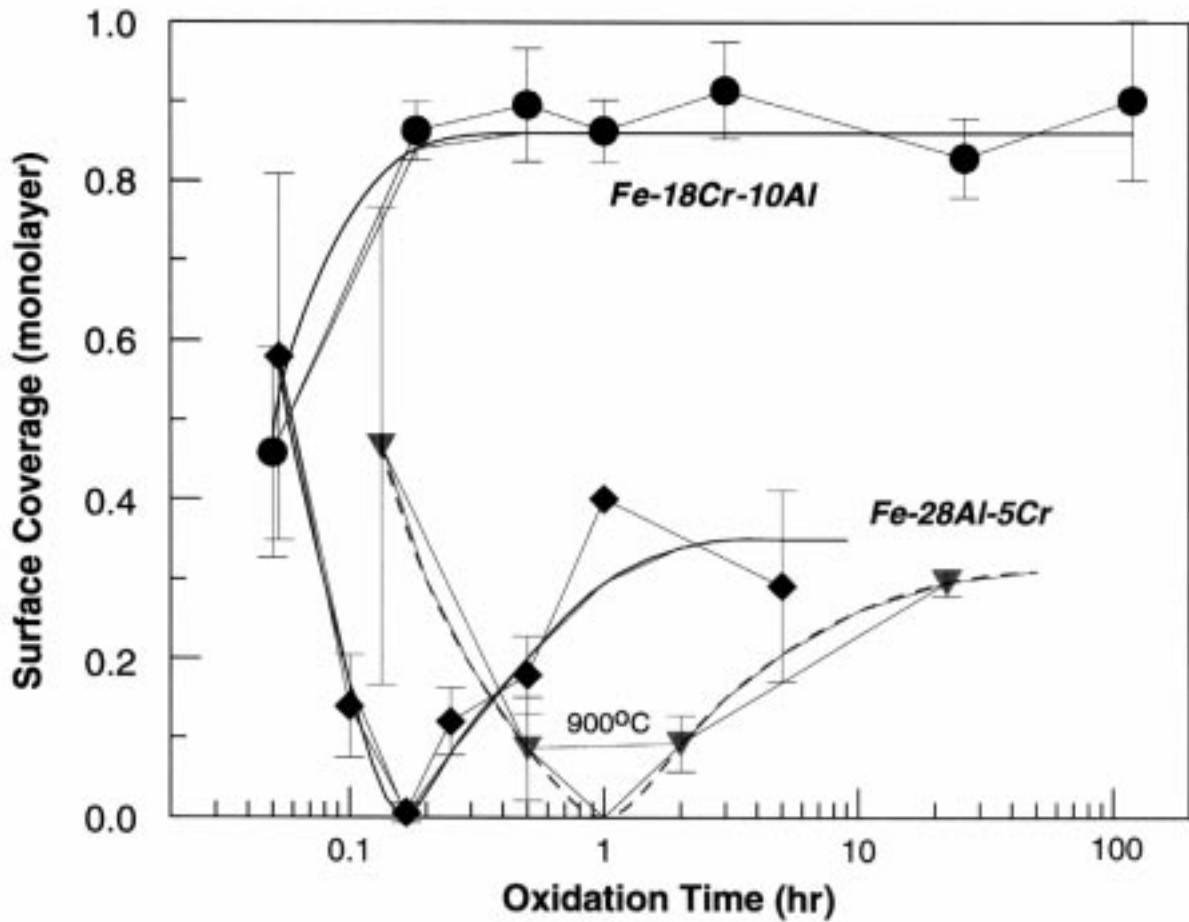
For the FeCrAl alloy, saturation of interfacial sulfur was reached after less than 10 minutes.

The rate was comparable to S diffusion in Fe, but the saturation concentration was significantly higher than the usual 0.25-0.5 monolayer coverage when S segregates to free surfaces of Fe or Ni single crystals. This high concentration may be related to a co-segregation effect of S with Cr, indicating some sulfide formation at the interface.

For the Fe₃Al, S was the only segregant at the scale/alloy interface, but its concentration changed nonmonotonically with time (oxide growth). The changes correlated with oxidation temperature, which is the major factor in affecting the film growth rate. This relationship strongly suggests that the equilibrium concentration of segregated S critically depends on oxide growth and type - the first- formed oxides are transitional δ -, θ - or γ - forms of alumina that then transform to α -Al₂O₃ with an expected loss of coherency at the Al₂O₃-metal interface. Such structural factors can be used to explain the complex time dependence of interfacial S segregation for the Fe₃Al system. At the same time, the monotonic increase in interfacial S for the FeCrAl alloy, as well as its higher concentration, can be related to the known faster transformation to α -Al₂O₃ on this substrate, as well as to the co-segregation of Cr.

Significance—This work demonstrates impurity segregation to dynamic Al₂O₃/alloy interfaces even for very thin and adherent films and also shows that the behavior is quite different from segregation to free surfaces. The research clearly points to the critical linked influences of substrate type, co-segregation behavior, film formation processes, and resulting interfacial structures in controlling sulfur segregation and associated oxide adherence.

Contact: Peggy Hou, Lawrence Berkeley National Laboratory
Phone: (510) 486-5560, Fax: (510) 486-4995, E-mail: pyhou@lbl.gov



Concentration of sulfur at Al_2O_3 -FeCrAl and Al_2O_3 -Fe3Al interfaces as a function of oxidation time at 1000°C. The dash line is for oxidation at 900°C. Sulfur segregation kinetics strongly depended on alloy being oxidized as well as the oxide growth rate and, by inference, the structural nature of the Al_2O_3 -metal interface.

Characterizing Impurities in Thin Film Silicon

*Scott McHugo, Al Thompson, and Gerry Lamble, Lawrence Berkeley Laboratory
H. Atwater, Claudine Chen, and R. Puglisi, California Institute of Technology*

Motivation—Low-cost photovoltaic silicon has a high concentration of impurities that limit cell performance. These impurities must be identified elementally and chemically before processes can be designed to remove them. Elemental identification and consideration of the diffusivity of the particular impurity provides vital information of time-temperature treatments required for impurity removal. Chemical identification is important for precipitated impurities because the chemical state significantly affects the rate of precipitate dissolution.

The Thin Film Si Team is studying several approaches for growing/depositing thin layers of Si on low-cost substrate. One approach is to deposit a-Si on a metal-coated glass with grain growth enhancements. NREL and Caltech are making such films. The NREL group uses optical excitation to alter the point defect dynamics while the Caltech group uses thermal annealing. The Caltech group utilizes regions of high Ni concentration, which controllably nucleate recrystallization sites and accelerate the recrystallization process. LBNL is applying synchrotron-based x-ray fluorescence analysis for characterization the Ni distribution and, more generally, to obtain elemental and chemical information on precipitated impurities.

Accomplishment—Studies on polysilicon have concentrated on determining which impurities are present, correlating the distribution of impurities with performance, identifying the chemical state of the impurities and measuring the thermal dissolution of the impurities. In these studies the LBNL group has identified transition metals, specifically Fe, Ni, Cr, Cu and Au as common contaminants which directly

correlate with poor cell performance (Fig. 1). The Fe contaminants are in a highly stable oxide/silicate state such that standard thermal processing will not allow for dissolution removal. These results are the first of their kind and lend great insight on how to improve the performance of polycrystalline silicon solar cells. Furthermore, studies have begun with Caltech on a-Si re-growth. Initial results (Fig. 2) indicate Ni is incorporated into the growing polysilicon but no agglomeration of Ni was detected at the amorphous/polysilicon interface. This provides insight into the mechanism for enhancement of recrystallization by the presence of Ni.

Significance—Because solar cell substrates typically contain high concentrations of metallic impurities, some impurities form precipitates which can act as degrading junction shunts. The chemical composition of such precipitates must be known before suitable gettering processes can be designed. This work has generated preliminary results suggesting possibilities of the presence of oxides or silicates of transition metals. Such oxides or silicates are difficult to dissolve by thermal processes and indicate that impurity removal after formation of such compounds is not feasible within solar cell processing parameters. Past studies revealed regions of low minority carrier diffusion lengths, and thus poor performance, even with application of processing treatments designed to remove metal impurities. Various explanations were suggested for this behavior, from intrinsic recombination activity of structural defects to the presence of SiC or SiO₂. The present results suggest that metal oxide or silicate precipitates may be the cause behind these persistently poor performance regions.

Contact: Scott McHugo, Lawrence Berkeley Laboratory
Phone: (510) 486-4874, Fax: (510) 486-7696, E-mail: samchogo@lbl.gov

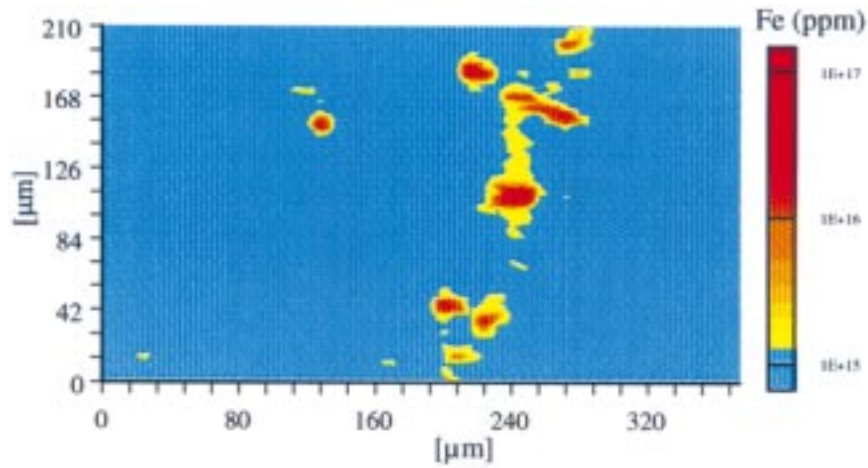


Figure 1. X-ray fluorescence (XRF) image of Fe distribution in polycrystalline silicon used for solar cells. A region of intense Fe concentration was analyzed with x-ray absorption spectromicroscopy and shown to be in an oxide or silicate state, which is highly stable and cannot be easily dissolved. In addition to Fe, Cr and Ni were observed in this sample at the same locations as the Fe.

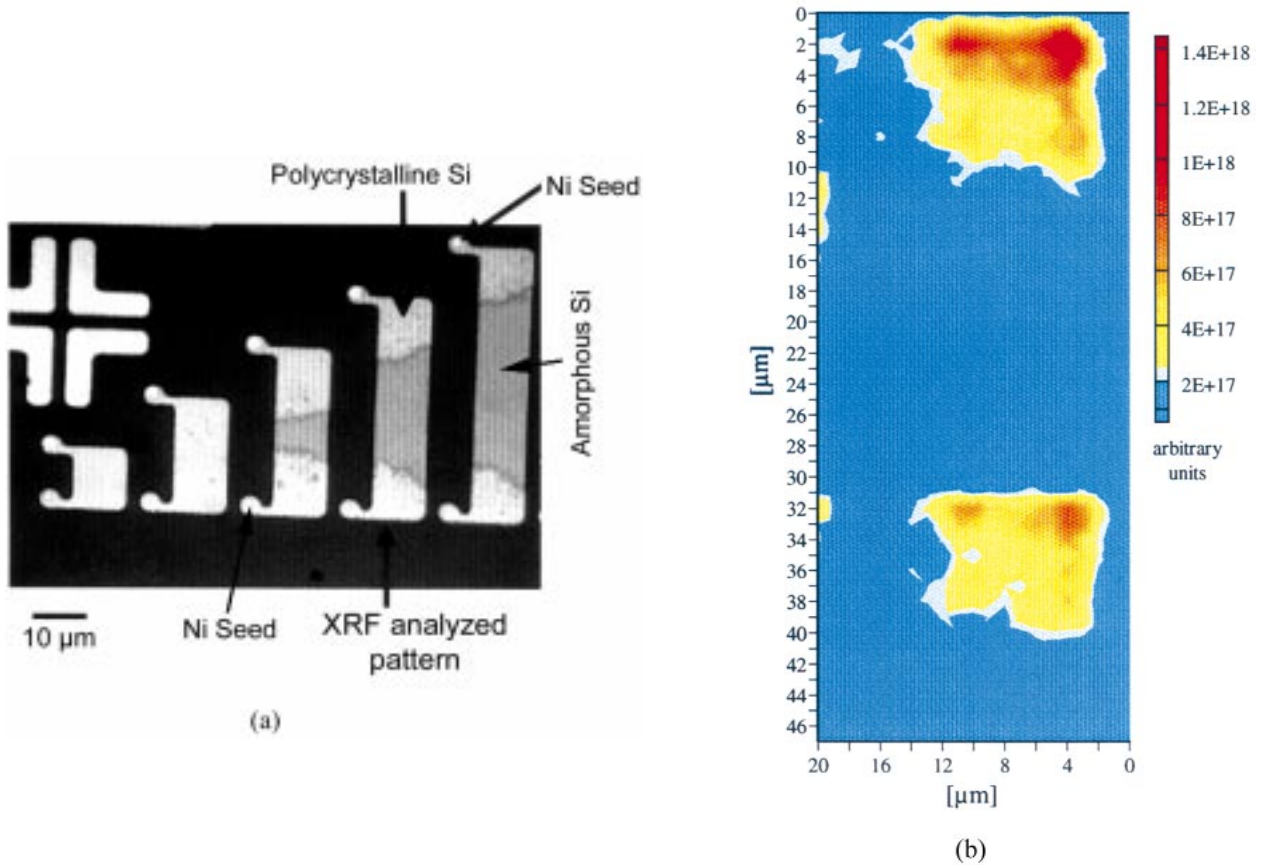


Figure 2a. Optical image of Ni seed-assisted polysilicon growth from amorphous silicon and (b) an XRF image of the Ni distribution. Note the presence of Ni in the polysilicon layer and the absence of accumulated Ni at the amorphous/polysilicon interface.

Ab Initio Studies of Point Defects and Dislocations in Si

*T. Lenosky, B. Sadigh, V. Bulatov and T. Diaz de la Rubia,
Lawrence Livermore National Laboratory*

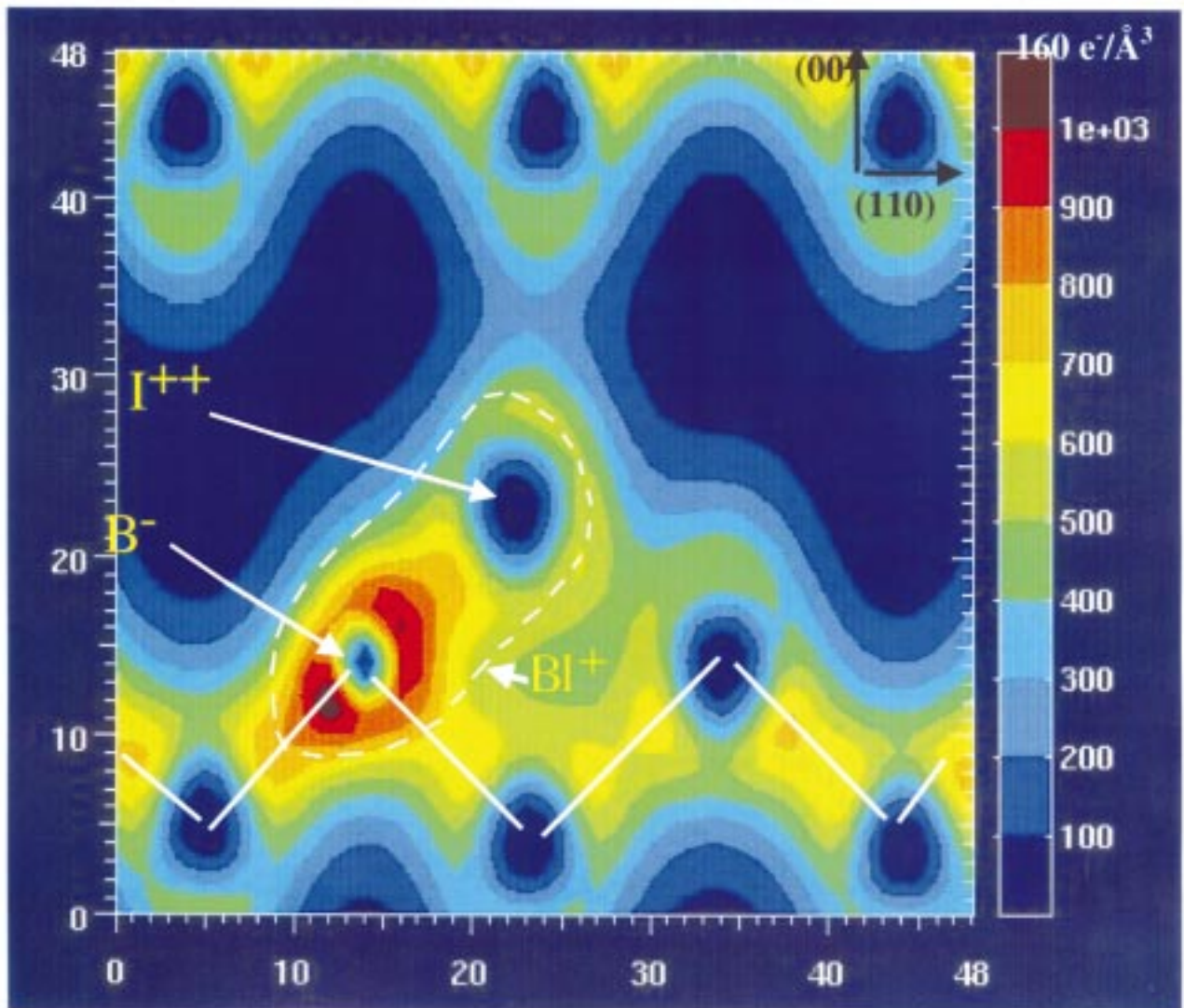
Motivation—Thin film solar cells based on silicon are a promising option for low-cost photovoltaics. A key research issue is the degradation of electronic properties due to the presence of atomic size as well as extended defects. Thus, it is important to understand the properties of vacancies, self-interstitials, and dislocations as well as how these defects interact with dopant atoms such as boron.

Accomplishment—We have investigated the mechanism of boron diffusion and clustering in silicon. We employ density functional theory within both the local-density and generalized gradient approximations using the VASP plane-wave pseudopotential code, with Vanderbilt ultrasoft pseudopotentials. All the boron and boron cluster calculations are represented by 64 atom supercells and were performed with a $2 \times 2 \times 2$ uniform grid of k-points. Both diffusion and clustering of B occur mainly due to the presence of excess self-interstitials (I^{++}) created by ion-implantation. These are highly mobile species and are thought to diffuse in a singly positive charge state. They are attracted to the negatively charged immobile B atoms (B^-) present at the substitutional sites in the lattice. They subsequently form a mobile complex (BI^+) with a binding energy of 0.87 eV. The figure shows a 2-D cut through a 64 atom supercell in which a BI^+ complex has been introduced and relaxed to its lowest energy configuration. We demonstrated that boron diffuses via an interstitialcy mechanism through the hexagonal site in the lattice with activation energy of 0.63 eV. The diffusion of the complex is responsible for the unwanted spread of the dopants in Si, as well as the nucleation and growth of immobile and electrically inactive B-Si clusters.

We have investigated the formation volume of defects in Si and the atomic reconstruction at the core of dislocations as a first step toward understanding the role of stress on diffusion. We have found, surprisingly, that even a 256-atom cell is not large enough to fully contain the electronic eigenstates of the vacancy. In this cell, we calculate vacancy formation energy of 3.64 eV at the experimental lattice constant and 3.34 eV when the volume of the cell is allowed to relax. We find a migration barrier of 0.25 eV, and a negative formation volume of -7 \AA^3 , i.e., there is a net reduction in volume when a vacancy is formed by moving an atom to a surface.

For dislocations, it is expected that reconstruction of the core eliminates dangling bonds by dimerization resulting in energy gain. We calculated reconstruction energies of 0.42 eV/bond and 1.02 eV/bond for the 90° and 30° partials, respectively. Since dislocation motion in silicon is governed by double kink nucleation and migration processes, (related to the cost of bond breaking and reconstruction), the results indicate that the mobility of the 30° partial should be lower than that of the 90° partial, in excellent agreement with experimental observations.

Significance—Ab initio methods provide a powerful way to explore defect properties and their interaction with dopants in silicon. Specifically, we have demonstrated that boron diffuses in silicon via an interstitialcy mechanism and calculated the local distortion field and the relaxation volume of the vacancy in silicon as well as the reconstruction energy per bond at the core of partial dislocations. The technological impact will stem from putting this fundamental knowledge to use in improving solar cells.



The figure shows the relaxed atomic positions of a substitutional boron/silicon interstitial in a 64 atom silicon supercell. The color indicates local electronic density with red showing higher density of electrons than blue. The complex of a boron atom and a silicon self interstitial is bound by 0.87 eV.

Exciton Reduced Mass in InGaAsN Photovoltaic Materials

E. D. Jones, A. A. Allerman, S. R. Kurtz, and N. A. Modine
Sandia National Laboratories

Motivation—A new semiconductor alloy system, InGaAsN, is an important material for achieving the goal of this Center Project of multi-junction solar cells with efficiencies greater than 40%. The introduction of small amounts of nitrogen (~2 at.%) in the InGaAs alloy system greatly reduces the band gap energy, with reductions approaching 0.5 eV. The initial portion of this research program is thus aimed at understanding the fundamental nature of the effect of adding substitutional isoelectronic nitrogen atoms for arsenic. Besides the effect on the bandgap energy, of importance is what other material properties are strongly affected or modified by the introduction of a small amount of nitrogen into GaAs?

Accomplishment—A series of InGaAsN alloys with varying nitrogen concentrations with the indium content adjusted to provide lattice matched conditions were grown using metal organic chemical vapor deposition (MOCVD) reactors. In the first study we investigated the photoluminescence energy and line shape for varying growth conditions. Studies of the photoluminescence line width and intensity for these samples were performed in order to determine the optimum growth parameters and conditions. A typical 4-K photoluminescence spectrum for a 1% nitrogen sample is shown in Fig. 1. The experimental full-width-at-half-maximum (FWHM) line width is about 18 meV. An interpretation of this FWHM value in terms of alloys fluctuation theories can be used to infer the effective exciton mass to be about 0.10 which is to be compared with the pure GaAs value of 0.04. Our recent band structure calculations suggest that the reduction to the bandgap energy is a result of Γ -X and Γ -L mixing

between the GaAs conduction band states. With this strong mixing, we also expect mass changes.

In order to study the effect of mixing and the resultant change in mass, we measured the hydrostatic pressure dependence of the FWHM between ambient and 120 kbar with the result shown in Fig. 2. A miniature diamond anvil cell with helium as the pressure medium was used to produce hydrostatic pressures. Using the current theories for the photoluminescence line width based on alloy fluctuations the effective exciton mass can be inferred from the FWHM line width data shown in Fig. 2. Figure 3 shows the increase in the exciton effective mass as a function of pressure. This increase is a direct result of increased Γ -X mixing with pressure, and hence an increased mass change because of the heavy X-point mass. The current theoretical challenge is to accurately calculate the mass and its pressure dependence from a first principles approach. The latest calculations, showing good agreement with experiments, are also shown as stars in Fig. 3.

Significance—Calculations show that incorporating a 1 eV band gap material into existing GaAs-based multi-junction tandem solar cells can increase the overall solar cell efficiency by as much as 10%, with maximum theoretical efficiencies for the tandem cell greater than 40%. These increased efficiencies will lead to smaller (and lighter) solar cell panels especially important for spaced-based applications. The mass measurements will yield information regarding the ideal and actual values of the carrier mobilities for these kinds of solar cells.

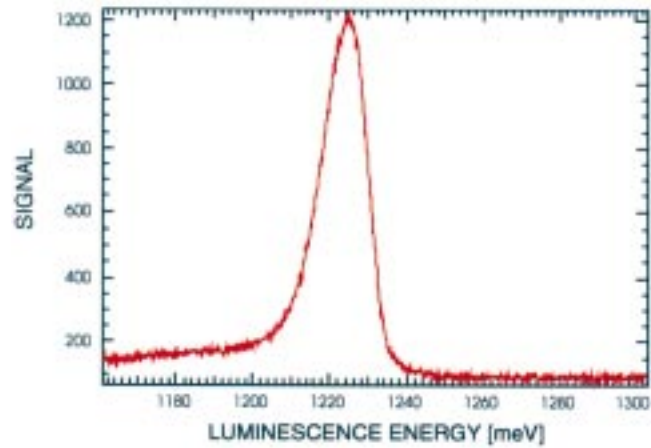


Figure 1. Low temperature (4K) photoluminescence spectrum for an InGaAsN (~1%N) epilayer film lattice matched to GaAs. The band gap energy is 1222 meV and the FWHM is about 18 meV.

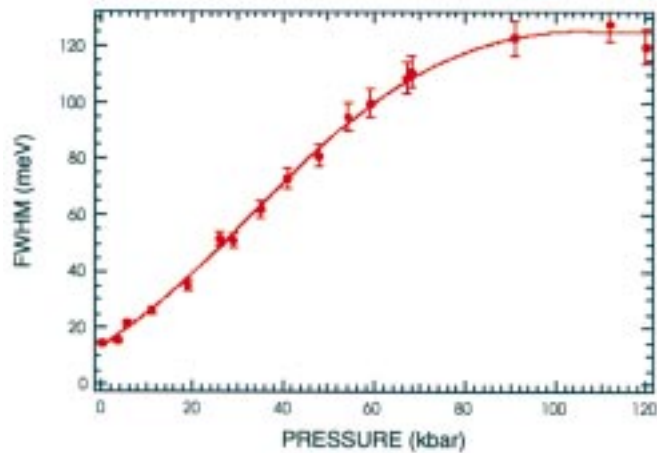


Figure 2. Pressure dependence of the FWHM line width for the sample in Fig. 1.

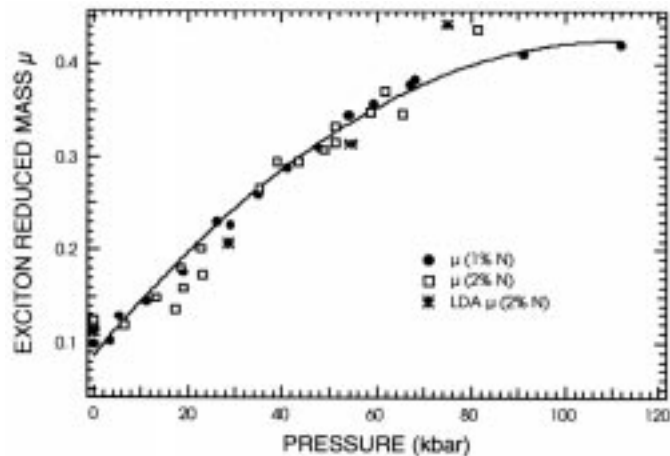


Figure 3. Pressure dependence of the exciton effective mass for 1 & 2% N InGaAsN alloy. The stars are calculations based on the LDA.

High-Temperature Mo-12Si-8.5B Intermetallics: Fatigue and Fracture Behavior at Ambient and Elevated Temperatures

H. Choe, D. Chen, and R. O. Ritchie *Lawrence Berkeley National Laboratory*
J. H. Schneibel, *Oak Ridge National Laboratory*

Motivation—There has been considerable effort to develop improved materials for structural use at temperatures $>1000^{\circ}\text{C}$, for such applications as advanced power turbines and reciprocating engines. One such system is molybdenum silicides which have excellent oxidation resistance up to 1700°C and relatively easy processibility; however, like most high melting point intermetallics, the toughness of these materials is unacceptably low. Boron-containing molybdenum silicides, are of interest due to their superior low-temperature “pest” resistance and comparable high temperature oxidation resistance to MoSi_2 -based silicides, but with somewhat improved mechanical properties. Our current focus is on Mo-Si-B multiphase intermetallic systems, which contain Mo, Mo_3Si , T1 (Mo_5Si_3), and T2 (Mo_5SiB_2) phases, with the objective of understanding the compositional, microstructural and mechanistic features that can induce optimal low-temperature toughness combined with high-temperature crack growth resistance, e.g., due to creep and fatigue. Here we report on a Mo-12Si-8.5B (at.%) alloy containing Mo, Mo_3Si , and T2 phases (microstructure in Figure 1) which is anticipated to have substantially higher fracture toughness than alloys from the Mo_3Si -T1-T2 system.

Accomplishment—The fracture toughness (Fig. 2) and fatigue-crack propagation resistance (Fig. 3) of the Mo-12Si-8.5B alloy are seen to be substantially higher than monolithic MoSi_2 and comparable with Nb-wire reinforced MoSi_2 composites. Indeed, although the resistance curve is not very steep, *intrinsic* fracture toughness values (at crack initiation where $\Delta a \rightarrow 0$) are $\sim 75\%$ higher than that of MoSi_2 at 25°C and a factor of $\sim 2\frac{1}{2}$ higher at 1200°C . Based on limited fractographic examination to date, this vastly

improved resistance to fracture appears to be associated with delamination and crack deflection at internal interfaces and with the superior mechanical properties of relatively ductile Mo phase. Corresponding fatigue-crack growth properties, (Fig. 3) are similarly far superior to that of monolithic MoSi_2 , with fatigue threshold values a factor of 4 times larger; moreover, cyclic fatigue resistance is further enhanced at 1200°C compared to room temperature. *Indeed, it is apparent that this alloy is essentially not susceptible to premature failure by fatigue.* There are good mechanistic reasons for this. Cyclic fatigue in brittle materials, e.g., ceramics and intermetallics, arises from a progressive degradation in extrinsic (resistance curve) toughening *behind* the crack tip. The Mo-12Si-8.5B alloy, however, is primarily toughened intrinsically, i.e., from an enhanced resistance to damage mechanisms *ahead* of the crack tip. Since there is only limited extrinsic toughening to degrade, these alloys show only minimal susceptibility to fatigue failure, which is the principal mode of *in service* failures in structural components.

Significance—The combination of a high fracture toughness ($>10 \text{ MPa}\sqrt{\text{m}}$) with a fatigue threshold of $7 \text{ MPa}\sqrt{\text{m}}$ at temperatures as high as 1200°C for the Mo-12Si-8.5B alloy is impressive for any high-temperature intermetallic system without (expensive) composite reinforcement. Future studies will focus on transmission and scanning electron microscopy to discern the salient mechanisms of toughness and high-temperature crack growth and to optimize microstructures and compositions for the best balance of mechanical properties. Powder-processing with varying α -Mo volume fractions to vary the morphology and continuity of the Mo phase will also be explored.

Contact: R. O. Ritchie, Lawrence Berkeley National Laboratory
Phone: (510) 486-5798, Fax: (510) 486-4995, E-mail: roritchie@lbl.gov

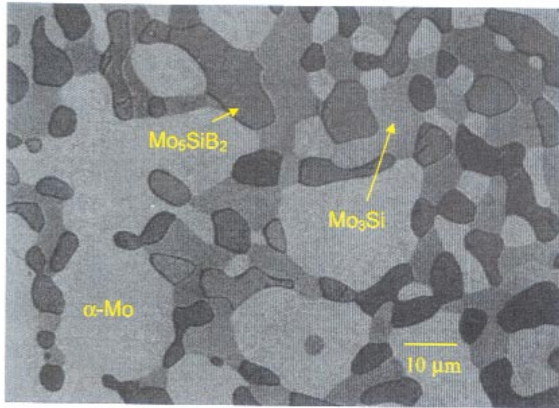


Figure 1. Scanning electron micrograph of Mo-12Si-8.5B alloy. The structure is etched with Murakami's reagent.

Figure 2. Resistance to fracture behavior of Mo-12Si-8.5B both at ambient and elevated temperatures, in comparison to previous results on monolithic and composite MoSi₂ alloys.

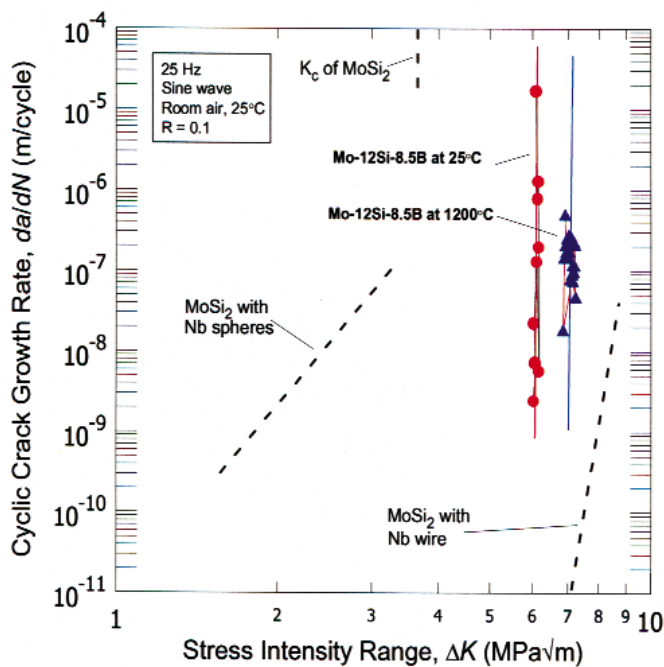
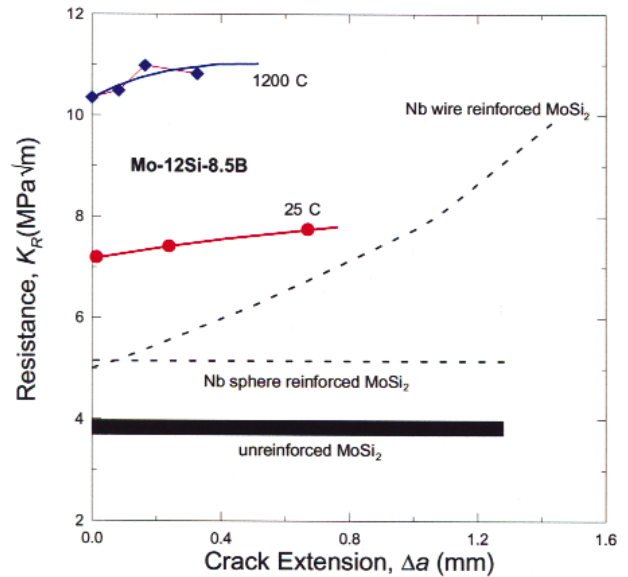


Figure 3. Cyclic fatigue-crack growth behavior of Mo-12Si-8.5B both at ambient and elevated temperatures, again compared to previous results on monolithic and composite MoSi₂ alloys.

Oxidation Behavior of Mo₅Si₃-Based Alloys

K. Natesan, Argonne National Laboratory

Motivation—High-temperature structural materials are critically needed to improve the thermal efficiency and reliability of energy conversion systems. Currently available alloys, such as Ni-base single-crystal superalloys, are limited to temperatures of ~1100°C. Many applications require temperature capabilities that exceed 1400°C. The melting temperature (T_m) of a material for structural applications at 1400°C should be >2000°C in order not to exceed 0.75 T_m during service and appreciable high-temperature strength is maintained. Of potential candidates, Mo silicides are particularly attractive because of their high melting points, high thermal and electrical conductivities, and mechanical strength. A key issue associated with these materials is resistance to oxidation at low temperatures. This task was initiated to evaluate the oxidation performance of Mo₅Si₃-based alloys over a wide temperature range and to establish a mechanistic understanding of the oxidation process.

Accomplishment—Oxidation studies were conducted on binary and several B-containing Mo₅Si₃ alloys in air at 500-1400°C. The alloys included single-crystal (SC) and hot-pressed polycrystalline Mo₅Si₃, Mo₅Si₃ with 2 at.% B (T1 phase), Mo₅SiB₂ (T2 phase), and Mo₅Si₃ with 7.2-9.3 at.% B. Oxidation products were characterized for microstructure, composition, and phase stability. Weight change data for the SC and T1 alloys showed rapid weight loss, indicating formation of volatile Mo oxide and no protection from silica (see Fig. 1). Figure 2 shows weight change data for the Mo₅Si₃ alloy containing 9.3 at.% B, when oxidized in air at 500-800°C. The data showed a protective scaling of the alloy at 500°C, not because of SiO₂ formation, but because the rate of volatilization

of Mo oxide is negligible. At 600°C, the alloy exhibited substantial weight loss after an initial weight increase for ~100 h. Oxidation at 700°C showed a sharp weight loss over a few hours of oxidation. Figure 3 shows SEM photomicrographs of specimens exposed in air for 0.5, 1.5, and 5 h at 700°C. After 0.5 h of exposure, the specimen showed a needlelike MoO₃ phase, and after 1.5 h, some consolidation was noted. After 5 h of exposure, the needlelike morphology had completely disappeared and the white spots on the surface were identified by energy-dispersive X-ray analysis as pure Mo, indicating direct oxidation of Mo₅Si₃ to Mo and SiO₂. The alloy undergoes nonprotective scaling at 700°C and has very little tendency to form either silica or borosilicate as a continuous scale to resist further oxidation. Oxidation of the alloy at 1000 and 1200°C showed a sharp drop in specimen weight for ~2 h, after which a plateau was reached and the weight then changed little during 50-70 h of additional exposure. The morphology of the scale observed after oxidation at 800°C consisted of light-colored MoO₂ phase and a dark gray Si-rich oxide. After oxidation at 1000 and 1200°C, the surface consisted of Si-rich oxide and almost pure Mo particles. The surface layer showed significant cracking and peeling and seemed to be highly plastic, as indicated by curling rather than spalling of the oxide layer.

Significance—Binary Mo silicides are prone to nonprotective oxidation at low temperatures (500-700°C) in air, primarily because the silica growth rates needed to form an external continuous scale are extremely low. Addition of B to accelerate formation of borosilicate at low temperatures is not proved. Thermal and mechanical stability of SiO₂ and/or borosilicate at T>1000°C need further investigation.

Contact: K. Natesan, Argonne National Laboratory

Phone: (630) 252-5103, Fax: (630) 252-3604, E-mail: natesan@anl.gov

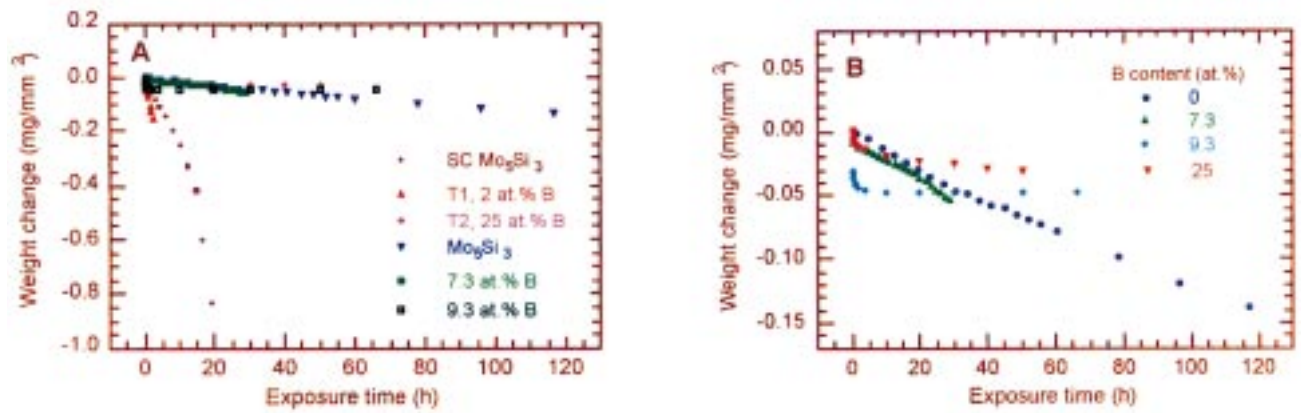


Figure 1. Thermogravimetric weight change data for (A) several alloys exposed to air at 800°C and (B) same data as in A, replotted without data for SC and T1 alloys.

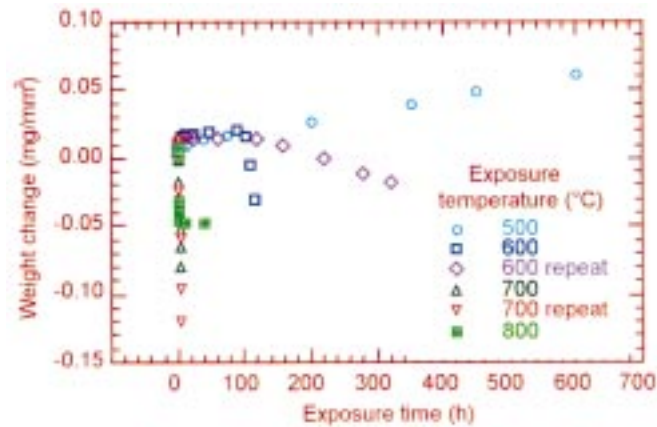


Figure 2. Thermogravimetric weight change data for Mo₅Si₃ alloy containing 9.3 at.% B, oxidized at 500, 600, 700, and 800°C.

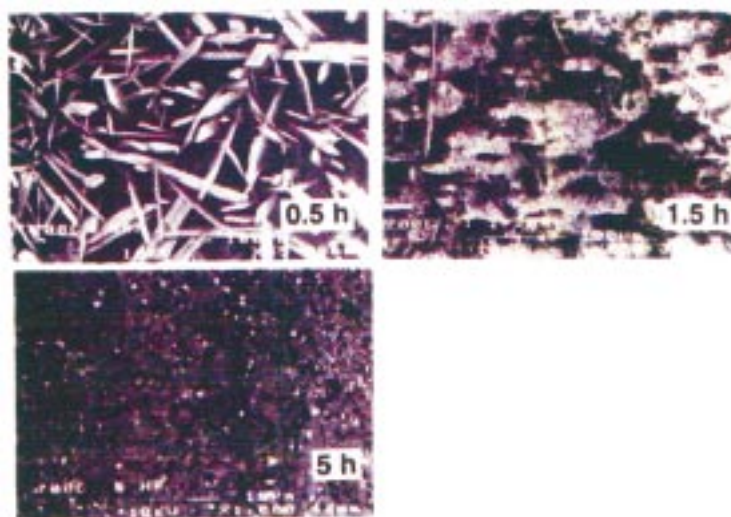
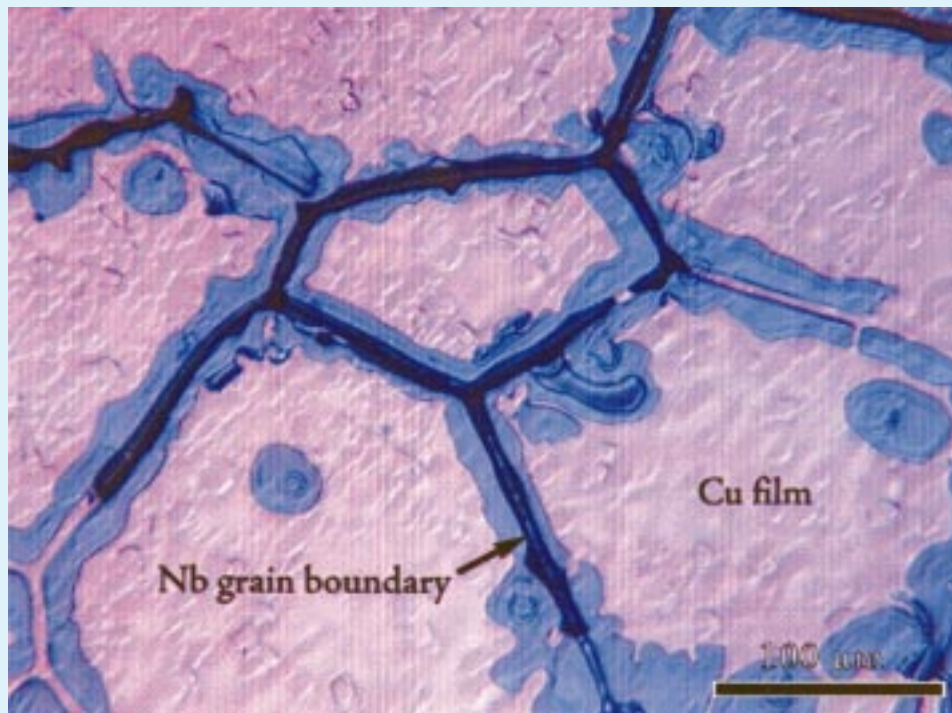


Figure 3. SEM photomicrographs of Mo₅Si₃ alloy containing 9.3 at.% B, after oxidation in air at 700°C for 0.5, 1.5, and 5 h.



The figures on the front and back covers relate to some of the accomplishments described in this issue of Research Briefs. The above figure illustrates the initial interfacial microstructure in the transient liquid metal joining of ceramics - using Cu/Nb/Cu multilayers. Controlled dewetting of the Cu at high temperatures produces strong Nb/alumina bonds. The figure on the front shows the mesh for 3-D finite element modeling of nanoindentation that takes into account of the actual indenter shape to quantify the mechanical properties of hard surface layers independently of those of soft substrates.

SAND2000-1348: Prepared by the DOE Center of Excellence for the Synthesis and Processing of Advanced Materials at Sandia National Laboratories, Albuquerque, New Mexico 87185 for the Division of Materials Sciences, Office of Basic Energy Sciences, U.S. Department of Energy. Sandia is a multiprogram laboratory operated by Sandia Corporation, A Lockheed Martin Company, for the Department of Energy under Contract No. DE-AC04-94AL85000.